Long-term variability in the El Niño/Southern Oscillation and associated teleconnections

MICHAEL E. MANN and RAYMOND S. BRADLEY

Department of Geosciences, University of Massachusetts
Amherst, Massachusetts 01003 U.S.A.

MALCOLM K. HUGHES

Laboratory of Tree Ring Research, University of Arizona
Tucson, Arizona 85721 U.S.A.

Abstract

We analyze global patterns of reconstructed surface temperature for insights into the behavior of the El Niño/Southern Oscillation (ENSO) and related climatic variability during the past three centuries. The global temperature reconstructions are based on calibrations of a large set of globally distributed proxy records, or "multiproxy" data, against the dominant patterns of surface temperature during the past century. These calibrations allow us to estimate large-scale surface temperature patterns back in time. The reconstructed eastern equatorial Pacific "Niño-3" areal-mean sea surface temperature (SST) index is used as a direct diagnostic of El Niño itself, while the global ENSO phenomenon is analyzed based on the full global temperature fields. We document low-frequency changes in the base state, amplitude of interannual variability, and extremes in El Niño, as well as in the global pattern of ENSO variability. Recent anomalous behavior in both El Niño and the global ENSO is interpreted in the context of the long-term reconstructed history and possible forcing mechanisms. The mean state of ENSO, its global patterns of influence, amplitude of interannual variability, and frequency of extreme events show considerable multidecadal and century-scale variability over the past several centuries. Many of these changes appear to be related to changes in global climate, and the histories of external forcing agents, including recent anthropogenic forcing.

Introduction

The instrumental record of roughly the past century provides many key insights into the nature of the global El Niño/Southern Oscillation (ENSO) phenomenon. For example, classic instrumental indices of ENSO, such as the Southern Oscillation Index (SOI) or Niño-3 eastern tropical Pacific sea surface temperature (SST) index, demonstrate concentration of interannual variability in the interannual 3–7 year period band, (2) interdecadal modulation in the frequency

and intensity of ENSO episodes, and (3) demonstrable (though variable) influences of ENSO on extratropical storm tracks influencing the climates of North America and other regions remote from the tropical Pacific (see, e.g., the reviews of Philander 1990; Diaz and Markgraf 1993; Allan et al. 1996; and references within). There is little instrumental evidence, however, to describe the nature of variability prior to the twentieth century. A variety of theoretical, dynamical models support most of the features of ENSO evident in the instrumental record, including the interannual band-limited characteristics of ENSO (e.g., Jin et al. 1994; Tziperman et al. 1994; Lau et al. 1992), the tendency for amplitude and frequency modulation on longer timescales (either naturally—e.g., Zebiak and Cane 1991; Knutson et al. 1997—or due to "external" forcing of the tropical coupled ocean-atmosphere system—e.g., Zebiak and Cane 1987), and the characteristic influences on extratropical atmospheric circulation and associated climate variability (e.g., Lau and Nath 1994). Such theoretical models, however, have a considerable number of assumptions (i.e., parameterizations) of the modern climate built into them. There thus remains considerable uncertainty as to how ENSO has varied in past centuries, and, just as important, how ENSO *ought to* vary on long timescales (due either to external climate forcing or to low-frequency internal variability) given the limitations of our current theoretical understanding of the governing dynamics.

Trends in ENSO, and the dynamics or forcings governing them, are in fact uncertain even for the past century. The instrumental record of tropical Pacific SST is sparse during the early half of the twentieth century, and depending on how one assesses the instrumental record, quite remarkably, both negative (i.e., La Niña-like) and positive (i.e., El Niño–like) significant trends can be argued for (see, e.g., Cane et al. 1997 and Meehl and Washington 1996, respectively). Furthermore, theoretical coupled models variously support both a negative (Cane et al. 1997) and a positive (e.g., Meehl and Washington 1996; Knutson et al. 1998) response of eastern tropical Pacific SST to anthropogenic greenhouse forcing. Conflicting interpretations of the observational record can be understood in terms of the competing influences of two prominent patterns of global surface temperature variability (Mann et al. 1998a) which include a globally synchronous large-scale warming trend and a regionally heterogeneous trend describing offsetting cooling in the tropical Pacific. The competition between these two large-scale trends complicates the interpretation of ENSO in terms of simple (e.g., the Niño-3) standard indices, and underscores the importance of understanding possible anthropogenic-related trends in the context of low-frequency natural variability. Aside from being too short to understand possible twentieth-century trends in an appropriate context, the observational record is also too brief to settle fundamental questions regarding the proper paradigm (e.g, stochastically forced linear oscillator vs. self-sustained nonlinear oscillator) for the dynamics which govern ENSO variability (Jin et al. 1994; Tziperman et al. 1994; Chang et al. 1996). Furthermore, questions regarding how unusual recent anomalous ENSO episodes may be (e.g., Trenberth and Hoar 1996, 1997; Rajagopalan et al. 1997), remain moot in the context of the insufficient length of the instrumental record. Limited evidence for nonstationary characteristics in extratropical teleconnection patterns of ENSO during the twentieth century (Cole and Cook 1997), too, is difficult to evaluate without a longer-term perspective on interdecadal and longer-term variability in the global ENSO phenomenon.

Proxy climate records stand as our only means of assessing the long-term variability associated with ENSO and its global influence. Several recent studies have demonstrated the potential for reconstructing ENSO-scale variability before the past century. The historical chronology of Quinn and Neal (1992, henceforth "QN92") provides some documentary evidence for the timing of warm episodes during the past few centuries, but the rating is qualitative and one-

sided (only warm, and not cold, events are indicated), and the reliability of the record is questionable more than a century or two back (an updated version of this chronology is provided by Ortlieb, this volume). Tropical and subtropical ice core records (Thompson 1992) can provide some inferences regarding ENSO variability, but the amount of variance explained is quite modest. Coral-based isotopic indicators of eastern tropical Pacific SST (e.g., Dunbar et al. 1994) or central tropical Pacific variability in precipitation (Cole et al. 1993) have provided site-based reconstructions of ENSO during past centuries, but these records are either too short (e.g., Cole et al. 1993) or too imperfectly dated (e.g., Dunbar et al. 1994) to provide a true year-by-year assessment of ENSO events in past centuries. A number of dendroclimatic (tree-ring-based) reconstructions of the SOI have been performed, based on dendroclimatic series in ENSO-sensitive regions such as western North America (Lough 1991; Michaelsen 1989; Michaelsen and Thompson 1992; Meko 1992; Cleaveland et al. 1992), combined Mexican/southwestern U.S. latewood density (Stahle and Cleaveland 1993), and combinations of tropical Pacific and North American chronologies (Stahle et al. 1998). While such reconstructions can provide long-term descriptions of interannual ENSO-related climate variability, variations on longer timescales (i.e., greater than several decades) are often limited by removal of non-climatic tree growth trends, and variations at shorter timescales (i.e., year-to-year variations) by the nontrivial biological persistence implicit to tree growth. Reliance on purely extratropical dendroclimatic networks, moreover, assumes a "stationarity" in the extratropical response to tropical ENSO events which may not be warranted (e.g., Meehl and Branstator 1992).

An alternative approach to ENSO reconstruction employs a network of diverse, globally distributed, high-resolution (i.e., seasonal or annual) proxy indicators or a "multiproxy" network (Bradley and Jones 1993; Hughes and Diaz 1994; Diaz and Pulwarty 1994; Mann et al. 1995; Barnett et al. 1996). Through exploiting the complementary information shared by a wide network of different types of proxy climate indicators, the multiproxy approach to climatic reconstruction diminishes the impact of weaknesses in any individual type or location of indicator, and makes use of the mutual strength of diverse data. We make use of recent global temperature reconstructions which are based on the calibration of multiproxy data networks against the twentieth-century instrumental record of global surface temperatures. Details regarding the global pattern reconstructions and the underlying multiproxy data network (Mann et al. 1998a, henceforth "MBH98"; Mann et al. 1998b,c; Jones 1998), the evidence for external climate forcings in the reconstructed climate record (MBH98), and the patterns of variability in the North Atlantic and their relationships to coupled ocean-atmosphere model simulations (Delworth and Mann 1998) are provided elsewhere. Here we report findings from these reconstructions regarding long-term variability in ENSO and its large-scale patterns of influence. An attempt is made to separately assess the true, tropical ENSO phenomenon, and its potentially more tenuous extratropical influences through the use of distinct tropical (or, predominantly tropical) and global multiproxy networks. Though not without certain limitations, the reliability of the climate reconstructions is established through independent cross-validation and other internal consistency checks. With these reconstructions, we are able to take a global view of ENSO-related climate variability several centuries back in time. We examine questions of how the baseline state of ENSO has changed on long (multidecadal and century) timescales, how interannual variability associated with ENSO has been modulated on long timescales, and how global patterns of influence of El Niño may have changed over time.

In the second section, we describe the data used in this study, both proxy and instrumental, in more detail. In the third section, we describe the multiproxy pattern reconstruction approach

which forms the basis of our climate reconstructions. We describe separate applications of the approach to annual-mean reconstruction of both global surface temperature patterns and the more regional Niño-3 index of ENSO-related tropical surface temperature variations. In the fourth section, we discuss the global temperature and Niño-3 reconstructions, and analyze these reconstructions for low-frequency variability in ENSO and its global patterns of influence. We present our conclusions in the fifth section.

Data

We employ a multiproxy network consisting of diverse high-quality annual resolution proxy climate indicators and long historical or instrumental records collected and analyzed by many different paleoclimatologists (details provided in Table 1). All data have annual resolution (or represent annual means in the case of instrumental data available at monthly resolution). Small gaps were interpolated and any records which terminate slightly before the end of the 1902–80 calibration interval (see "Method") are extended by using persistence to 1980. Certain sub-networks of the full multiproxy data network (e.g., regional dendroclimatic networks) have been represented by a smaller number of their leading principal components (PCs), the maximum number of which (available back to 1820) is indicated in parentheses, to ensure a more regionally globally homogenous network. Two different sets of calibration experiments are performed. The first set uses the entire global multiproxy network (Fig. 1; this is essentially the same network used by MBH98) to reconstruct the "global ENSO" signal, while a more restricted "tropical" network (Fig. 2) of indicators in tropical regions or subtropical regions most consistently impacted by ENSO is used to reconstruct the specific tropical Pacific El Niño signal. In using largely independent networks to describe both the global ENSO and the tropical El Niño signals, we are able to independently assess both the tropical and global ENSO histories. We thereby in large part avoid the potentially flawed assumption of a stationary extratropical response to tropical ENSO forcing.

Table 1 Proxy, historical, and long instrumental data records used. Entries give description/type of record, location (latitude, longitude), meteorological variable indicated (or most likely indicated), beginning year (A.D.) of record, whether record is used in "tropical" ("trop") sub-network, and reference.

Record	Variable	Lat	Lon	Begin	Trop	Reference
1. Gridded temperature	Temp	42.5 N	92.5 W	1820		Jones and Bradley 1992
2. "	Temp	47.5 N	2.5 E	1757		
3. "	Temp	47.5 N	7.5 E	1753		"
4. "	Temp	47.5 N	12.5 E	1767		"
5. "	Temp	47.5 N	12.5 E	1775		"
6. "	Temp	52.5 N	17.5 E	1792		"
7. "	Temp	57.5 N	17.5 E	1756		"
8. "	Temp	57.5 N	17.5 E	1752		"
9. "	Temp	62.5 N	7.5 E	1816		"
10. "	Temp	62.5 N	12.5 E	1761		"
11. "	Temp	62.5 N	42.5 E	1814		"
12. Gridded precip	Precip	12.5 N	82.5 E	1813	x	"
13. "	Precip	17.5 N	72.5 W	1817	x	"
14. "	Precip	37.5 N	77.5 W	1809		"
15. "	Precip	42.5 N	2.5 E	1749		"
16. "	Precip	42.5 N	7.5 E	1804		"
17. "	Precip	42.5 N	7.5 E	1770		"
18. "	Precip	42.5 N	7.5 E	1813		"
19. "	Precip	42.5 N	7.5 E	1805		"
20. "	Precip	42.5 N	7.5 E	1697		"

Table 1 (Continued) Proxy, historical, and long instrumental data records used. Entries give description/type of record, location (latitude, longitude), meteorological variable indicated (or most likely indicated), beginning year (A.D.) of record, whether record is used in ”tropical” (”trop”) sub-network, and reference.

Record	Variable	Lat	Lon	Begin	Trop	Reference
21. ”	Precip	42.5 N	7.5 E	1809		”
22. ”	Precip	42.5 N	7.5 E	1785		”
Historical						
23. Cent England temp	Temp	52 N	0 E	1730		Manley 1959
24. Cent Europe temp	Temp	45 N	10 E	1550		Pfister 1992
Coral						
25. Burdekin River (fluoresc)	Precip/runoff	20 S	147 E	1746	x	Lough 1991
26. Galapagos Isabel Island ($d^{18}O$)	SST	1 S	91 W	1607	x	Dunbar et al. 1994
27. Gulf of Chiriqui, Panama ($d^{18}O$)	Precip	7.5 N	81 W	1708	x	Linsley et al. 1994
28. Gulf of Chiriqui, Panama (d^{18} C)	Ocean circ				x	
29. Espiritu Santu ($d^{18}O$)	SST	15 S	167 E	1806	x	Quinn et al. 1993
30. New Caledonia ($d^{18}O$)	SST	22 S	166 E	1658	x	Quinn et al. 1996
31. Great Barrier Reef (band thickness)	SST	19 S	148 E	1615	x	Lough, pers. comm.
32. Red Sea ($d^{18}O$)	SST/precip	29.5 N	35 E	1788	x	Heiss 1994
33. Red Sea ($d^{18}C$)	Ocean circ				x	
Ice Core						
34. Quelccaya summit ice core ($d^{18}0$)	(Air temp)	14 S	71 W	470	x	Thompson 1992
35. Quelccaya summit ice core (accum)	Precip			488	x	”
36. Quelccaya ice core 2 ($d^{18}O$)	(Air temp)			744	x	”
37. Quelccaya ice core 2 (accum)	Precip				x	”
38. Dunde ice core ($d^{18}O$)	(Air temp)	38 N	96 E	1606	x	Thompson 1992
39. Southern Greenland ice core (melt)	Summer temp	66 N	45 W	1545		Kameda et al. 1996
40. Svalbard ice core (melt)	Summer temp	79 N	17 W	1400		Tarussov 1992
41. Penny ice core ($d^{18}O$)	(Air temp)	70 N	70 W	1718		Fisher et al. 1998
42. Central Greenland stack ($d^{18}O$)	(Air temp)	77 N	60 W	553		Fisher et al. 1996
Dendroclimatic						
43. Upper Kolyma River (ring widths)	Temp	68 N	155 E	1550		Schweingruber, pers. comm.
44. Java teak (ring widths)	Precip	8 S	113 E	1746	x	Jacoby and D'Arrigo 1990
45. Tasmanian Huon Pine (ring widths)	Temp	43 S	148 E	900	x	Cook et al. 1991
46. New Zealand S. Island (ring widths)	Temp	44 S	170 E	1730	x	Norton and Palmer 1992
47. Central Patagonia (ring widths)	Temp	41 S	68 W	1500	x	Boninsegna 1992
48. Fernoscandian Scots Pine (density)	Temp	68 N	23 E	500		Briffa et al. 1992a
49. Northern Urals (density)	Temp	67 N	65 E	914		Briffa et al. 1995
50. Western North America (ring widths)	Temp	39 N	111 W	1602		Fritts and Shao 1992
51. North American tree line (ring widths)	Temp	69 N	163 W	1515		Jacoby and D'Arrigo 1989
52. ”	Temp	66 N	157 W	1586		”
53. ”	Temp	68 N	142 W	1580		”
54. ”	Temp	64 N	137 W	1459		”
55. ”	Temp	66 N	132 W	1626		”
56. ”	Temp	68 N	115 W	1428		”
57. ”	Temp	64 N	102 W	1491		”
58. ”	Temp	58 N	93 W	1650		”
59. ”	Temp	57 N	77 W	1663		”
60. ”	Temp	59 N	71 W	1641		”
61. ”	Temp	48 N	66 W	1400		”
62. S.E. U.S., N. Carolina (ring widths)	Precip	36 N	80 W	1005	x	Stahle et al. 1988
63. S.E. U.S., S. Carolina (ring widths)	Precip	34 N	81 W	1005	x	”
64. S.E. U.S., Georgia (ring widths)	Precip	33 N	83 W	1005	x	”
65. Mongolian Siberian Pine (ring widths)	Precip	48 N	100 E	1550	x	Jacoby et al. 1996
66. Yakutia (ring widths)	Temp	62 N	130 E	1400		Hughes et al. 1998
67. OK/TX U.S. ring widths (PC #1)	Precip	29–37 N	94–99 W	1600	x	Stahle and Cleaveland 1993
68–69. OK/TX U.S. ring widths (PC #2,3)	Precip	29–37 N	94–99 W	1700	x	”
70. S.W. U.S./Mex widths (PC #l)	Precip	24–37 N	103–109 W	1400	x	”
71. S.W. U.S./Mex widths (PC #2)	Precip	24–37 N	103–109 W	1500	x	”
72–73. S.W. U.S./Mex widths (PC #3,4)	Precip	24–37 N	103–109 W	1600	x	”
74–76. S.W. U.S./Mex widths (PC #5–7)	Precip	24–37 N	103–109 W	1700	x	”
77–78. S.W. U.S./Mex widths (PC #8,9)	Precip	24–37 N	103–109 W	1700	x	”
79. Eurasian tree line ring widths (PC #1)	Temp	60–70 N	100–180 E	1450		Vaganov et al. 1996
80. Eurasian tree line ring widths (PC #2)	Temp	60–70 N	100–180 E	1600		”
81. Eurasian tree line ring widths (PC #3)	Temp	60–70 N	100–180 E	1750		”

Table 1 (Continued) Proxy, historical, and long instrumental data records used. Entries give description/type of record, location (latitude, longitude), meteorological variable indicated (or most likely indicated), beginning year (A.D.) of record, whether record is used in ”tropical” (”trop”) sub-network, and reference.

Record	Variable	Lat	Lon	Begin	Trop	Reference
82–84. Aust/NZ chronologies (PC #1–3)	Mixed	37–42 S	145–175 E	1600	x	1TRDB[1]
85. Aust/NZ chronologies (PC #4)	Mixed	37–44 S	145–175 E	1750	x	”
86–88. S. American chronologies (PC #1–3)	Mixed	37–49 S	68–72 W	1600	x	”
89–94. N. American chronologies (PC #1–6)	Mixed	24–66 N	70–16O W	1400		”
95. N. American chronologies (PC #7)	Mixed	24–66 N	70–16O W	1600		”
96–97. N. American chronologies (PC #8,9)	Mixed	24–66 N	70–16O W	1750		”
98–115. Miscellaneous chronologies	Mixed	Global	Global	<1820		”

[1]Records taken from the International Tree Ring Data Bank (ITRDB). Full references are available through the website sponsored by the National Geophysical Data Center (NGDC): *http://julius.ngdc.noaa.gov/paleo.treering.html*

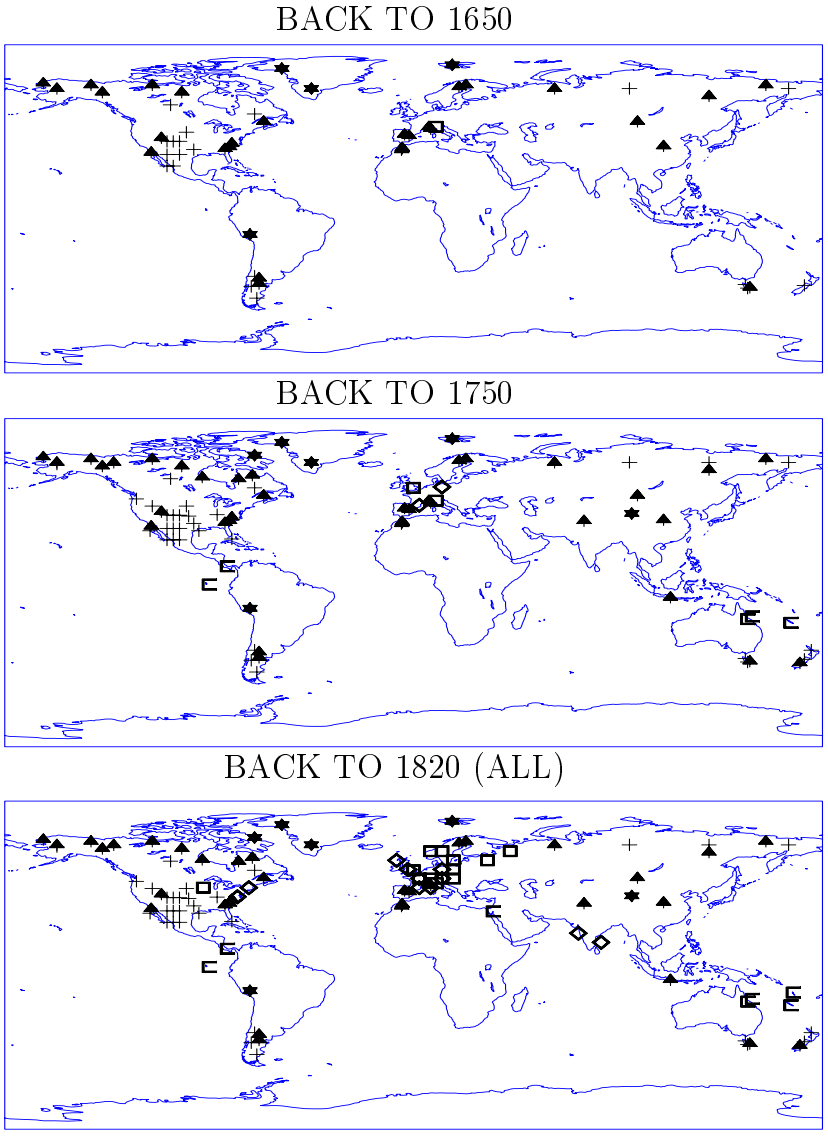

Fig. 1 Distribution of multiproxy network back to (a) 1650, (b) 1750, and (c) 1820 (all proxy indicators). Squares denote historical and instrumental temperature records; diamonds denote instrumental precipitation records; umbrella, or “tree,” symbols denote dendroclimatic indicators; and “C” symbols indicate corals. Groups of “+” symbols indicate PCs of dense tree-ring sub-networks, with the number of such symbols indicating the number of PCs. have been used to represent a dense regional dendroclimatic network. Certain sites (e.g., the Quelccaya ice core; see Table 1) consist of multiple proxy indicators (e.g., multiple cores, and both $d^{18}O$ isotope and accumulation measurements).

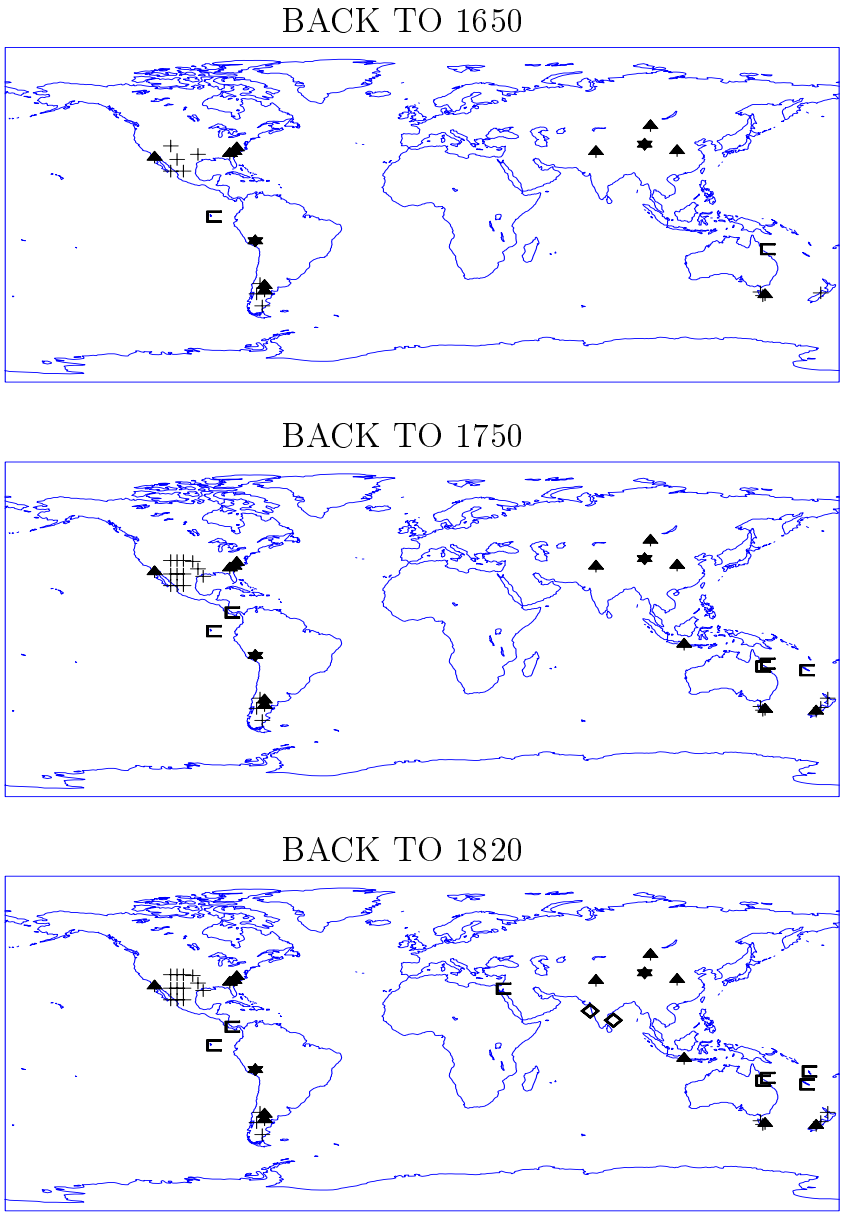

Fig. 2 Distribution of restricted multiproxy network used for Niño-3 reconstruction back to (a) 1650, (b) 1750, (c) 1820. Symbols as in Figure 1.

While a diverse and widely distributed set of independent climatic indicators can more faithfully capture a consistent climate, reducing the compromising effects of biases and weaknesses in the individual indicators, certain limitations must be carefully kept in mind in building an appropriate network. Dating errors in a given record (e.g., miscounted annual layers or rings) predating the calibration period can be problematic. It is well known that standardization by estimated non-climatic tree growth trends, and the limits of maximum segment lengths in dendroclimatic reconstructions, can strongly limit the maximum timescale climatic trends that are resolvable (Cook et al. 1995). We have, however, employed a careful screening of the dendroclimatic network to ensure conservative standardization procedures and long constituent

segment lengths, and variations on century and even multiple-century timescales are resolved typically. An analysis of the resolvability of multicentury timescale trends in these data and implications for long-term climate reconstruction is provided elsewhere (Mann et al. 1998b).

To calibrate the multiproxy networks, we make use of all available grid point (5 longitude by 5 latitude) land air and sea surface temperature anomaly data (Jones and Briffa 1992) with nearly continuous monthly sampling back to at least 1902. Short gaps in the monthly instrumental data are filled by linear interpolation. For the global temperature pattern reconstructions, we use all (M = 1082) available nearly continuous grid point data available back to 1902. For tropical Pacific SST/Niño reconstructions, we use the available M = 121 SST grid point data in the tropical Pacific region bounded by the two tropics and the longitudes 115°E to 80°W. These data are shown in Figure 3. Although there are notable gaps in the spatial sampling, significant enough portions of the globe are sampled to estimate (in the case of the global field) the Northern Hemisphere (NH) mean temperature series, and in both cases, the Niño-3 index of the El Niño phenomenon. Northern Hemisphere temperature is estimated as areally weighted (i.e., cosine latitude) averages over the Northern Hemisphere. The Niño-3 eastern equatorial Pacific SST index is constructed from the 10 grid points available over the conventional Niño-3 box (see Fig. 3) for the region 5ºS to 5ºN, 90ºW to 150ºW. While this spatial sampling covers only about one-third of the total Niño-3 region, the associated time series is nearly identical to the fully sampled Niño-3 region time series available (both series share 90% of their variance in common during their overlap back to 1953). The (negative) correlation of our Niño-3 average with the SOI—an alternative ENSO indicator which tends to covary oppositely with El Niño—is consistently high ($r^2 \approx 0.5$) and robust throughout the twentieth century for the intervals during which both are available ($0.44 \leq r^2 \leq 0.51$ for each of the 1902–49, 1950–80, 1950–93, and 1902–93 intervals). We thus assert that the sparser early grid point SST data in the eastern tropical Pacific are sufficient for a reliable Niño-3 index back to at least 1902.

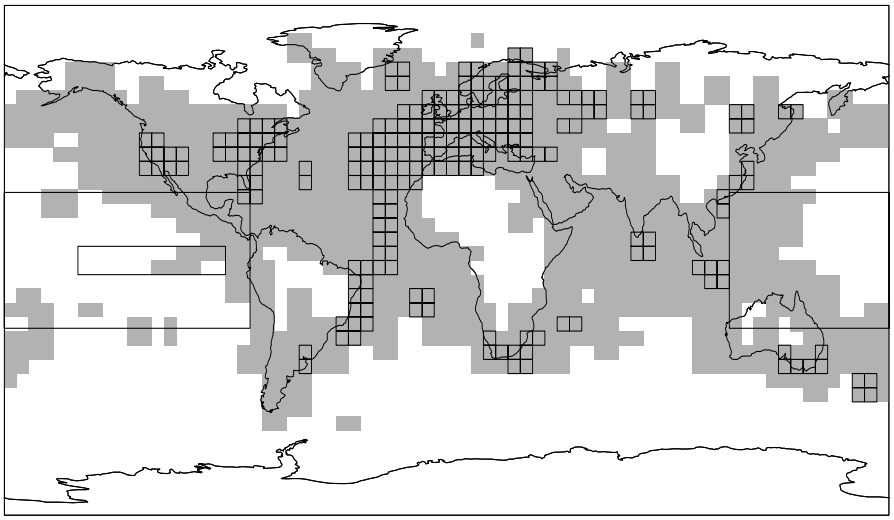

Fig. 3 Distribution of the (1082) nearly continuous available land air/sea surface temperature grid point data available from 1902 onward, indicated by shading. The squares indicate the subset of 219 grid points, with nearly continuous records extending back to 1854 that are used for verification. Northern Hemisphere (NH) and global (GLB) mean temperature are estimated as areally weighted (i.e., cosine latitude) averages over the Northern Hemisphere and global domains, respectively. The large rectangle indicates the tropical Pacific sub-domain discussed in the text. The small rectangle in the eastern tropical Pacific shows the traditional Niño-3 region. An arithmetic mean of grid point anomalies in our sampling of the Niño-3 region provides a reliable estimate of the fully sampled Niño-3 index (see text for discussion).

Method

The advantage of using multiproxy data networks in describing and reconstructing patterns of long-term climate variability has been discussed elsewhere (Bradley and Jones 1993; Hughes and Diaz 1994; Mann et al. 1995; Mann et al. 1998a,b,c) and relies upon the complementary characteristics and spatial sampling provided by a combined network of long historical and instrumental records, dendroclimatic, coral, and ice core–based climate proxy indicators of climate change. In our approach to climate field reconstruction, we seek to "train" the multiproxy network by calibrating it against the dominant patterns of variability in the modern instrumental record. In the case of the global temperature field reconstructions, we use the entire multiproxy network shown earlier in Figure 1, and we "train" this network by calibrating it, series-by-series, against the dominant global patterns of temperature variability using the full sampling of grid point data shown in Figure 3. In the case of Niño-3 index reconstruction, we use the restricted "tropical" multiproxy network (Fig. 2) and train it against the dominant patterns of SST variations confined to the tropical Pacific sub-domain (see region indicated in Fig. 3).

The calibration of the multiproxy network is accomplished by a multivariate regression against instrumental temperature data. Conventional multivariate regression approaches to paleoclimate reconstruction, such as canonical correlation analysis (CCA; see Preisendorfer 1988), which simultaneously decompose both the proxy "predictor" and instrumental "predictand" data in the regression process, work well when applied to relatively homogeneous networks of proxy data (e.g., regional dendroclimatic networks; see Cook et al. 1994 for an excellent review). However, we found that such approaches were not effective with the far more inhomogeneous multiproxy data networks. Different types of proxies (e.g., tree rings, ice cores, and historical records) differ considerably in their statistical properties, reflecting, for example, different seasonal windows of variability, and exhibiting different spectral attributes in their resolvability of climatic variations. Thus, rather than seeking to combine the disparate information from different proxy indicators initially through a multivariate decomposition of the proxy network itself, we instead choose to use the information contained in the network in a later stage of the regression process. Our approach is similar, in principle, to methods applied recently to the reconstruction of early instrumental temperature fields from sparse data, based on eigenvector interpolation techniques (Smith et al. 1996; Kaplan et al. 1998).

Our calibration approach, which was described in MBH98, is further detailed here. It involves first decomposing the twentieth-century instrumental surface temperature data into their dominant patterns of variability or "eigenvectors." Second, the individual climate proxy indicators are regressed against the time histories of these distinct patterns during their shared twentieth-century interval of overlap. One can think of the instrumental patterns as templates against which we "train" the much longer proxy "predictor." This calibration process allows us, finally, to solve an "inverse problem" whereby the closest-match estimates of surface temperature patterns are deduced back in time before the calibration period, on a year-by-year basis, based on information in the multiproxy network.

At least three fundamental assumptions are implicit in this approach. We assume (1) that the indicators in our multiproxy trainee network are statistically related to some linear combination of the eigenvectors of the instrumental global annual-mean temperature data. This assumption contrasts with that of typical paleoclimate calibration approaches. Rather than seeking, as in typical studies, to relate a particular proxy record locally to an at-site instrumental record of some *a priori* selected meteorological variable (e.g., temperature, precipitation, or atmospheric wind direction),

during some *a priori* selected seasonal (e.g., summer) window, we make instead a less restrictive assumption that whatever combination of local meteorological variables influence the proxy record, they find expression in one or more of the largest-scale patterns of annual climate variability. Ice core and coral proxy indicators reflect, in general, a variety of seasonal influences. Many extratropical tree-ring (ring widths and density) series primarily reflect warm-season temperature influences (see, e.g., Schweingruber et al. 1991; Bradley and Jones 1993). Tree-ring-width series in subtropical semiarid regions, however, are reflective in large part of cold-season precipitation influences. These influences are, in turn, tied to larger-scale atmospheric circulation variations (e.g., the PNA or NAO atmospheric patterns; see, e.g., D'Arrigo et al. 1993) that have important influences on large-scale temperature. When a proxy indicator represents some complex combination of local meteorological and seasonal influences, we make more complete use of the available information in the calibration process than do conventional approaches. While our method seeks only to recognize that variability in the proxy data tied to large-scale climatic patterns, it appears that temperature variability at interannual and longer timescales, for which the effective number of spatial degrees of freedom are greatly reduced (see, e.g., Jones and Briffa 1992), is inherently large-scale in nature. This latter observation underlies our assertion (2) that a relatively sparse but widely distributed sampling of long proxy and instrumental records may sample much of the large-scale variability that is important at interannual and longer timescales (see also Bradley 1996). Regions not directly represented in the trainee network may nonetheless be indirectly represented through teleconnections with regions that are. The El Niño/Southern Oscillation is itself an example of a pattern of climatic variability which exhibits global-scale influence (e.g., Halpert and Ropelewski 1992). Finally, we assume (3) that the patterns of variability captured by the multiproxy network have analogs in the patterns we resolve in the shorter instrumental data. This latter assumption represents a fairly weak stationarity requirement—we do not require that the climate itself be stationary. In fact, we expect that some sizable trends in the climate may be resolved by our reconstructions. We do, however, assume that the fundamental *spatial patterns* of variation which the climate has exhibited during the past century are similar to those by which it has varied during past recent centuries. Studies of instrumental surface temperature patterns suggest that such a form of stationarity holds up at least on multidecadal timescales, during the past century (Kaplan et al. 1998). Independent statistical cross-validation exercises and careful examination of the properties of the calibration residuals, as described later, provide the best evidence that these key assumptions hold, at least for the purposes of our reconstructions of temperature patterns during the past few centuries.

The first step in the pattern reconstruction process, as discussed above, is the decomposition of the modern instrumental data into its dominant spatiotemporal eigenvectors. The $N = 1104$ monthly samples available between 1902 and 1993 are sufficient for both the global temperature field (the $M = 1082$ grid point series described in the "Data" section; see Fig. 3) and the $M' = 121$ grid point series in the tropical Pacific region used in Niño-3 reconstruction, in providing a unique, well-posed eigendecomposition of the instrumental surface temperature data into its leading empirical eigenvectors. The method as described henceforth is understood to apply both the global pattern and tropical Pacific SST/Niño-3 reconstructions, which are performed independently.

For each grid point, the mean was removed, and the series was normalized by its standard deviation. The standardized data matrix can be written,

$$\underline{\mathbf{T}} = \begin{bmatrix} w_1 T_{t1}^{(1)} & w_2 T_{t1}^{(2)} \ldots w_M T_{t1}^{(M)} \\ w_1 T_{t2}^{(1)} & w_2 T_{t2}^{(2)} \ldots w_M T_{t2}^{(M)} \\ & \ldots \\ w_1 T_{tN}^{(1)} & w_2 T_{tN}^{(2)} \ldots w_M T_{tN}^{(M)} \end{bmatrix}$$

where $t_1, t_2, \ldots t_N$ spans over the N = 1104 months, and m = 1, 2, …, M spans the M = 1082 grid points. w_m indicates weighting by the cosine of the central latitude of each grid point to ensure that grid points contribute in proportion to the area represented.

A standard principal component analysis (PCA) is then applied to the standardized data matrix $\underline{T}$,

$$\underline{\mathbf{T}} = \sum_{k=1}^{K} \lambda_k u_k v_k$$

decomposing the data set into its dominant spatiotemporal eigenvectors. The M-vector or empirical orthogonal function (EOF) v_k describes the relative spatial pattern of the kth eigenvector, the N-vector u_k or PC describes its variation over time, and the scalar l_k describes the associated fraction of resolved (standardized and weighted) data variance.

The first five eigenvectors of the global temperature data are particularly important in the global temperature pattern reconstructions, as is described later. The EOFs (Fig. 4) and PCs (Fig. 5) are shown for these five eigenvectors, in decreasing order of the variance they explain in the global instrumental temperature data shown in Figure 3 (1 = 12%, 2 = 6.5%, 3 = 5%, 4 = 4%, 5 = 3.5%). The first eigenvector describes much of the variability in the global (GLB = 88%) and hemispheric (NH = 73%) means, and is associated with the significant global warming trend of the past century (see Fig. 5). Subsequent eigenvectors, in contrast, describe much of the spatial variability relative to the large-scale means (i.e., much of the remaining multivariate variance "MULT"). The second eigenvector is the dominant ENSO-related component of the global temperature data, describing 41% of the variance in the Niño-3 index, and exhibiting certain classic extratropical ENSO signatures (e.g., the "horseshoe" pattern of warm and cold SST anomalies in the North Pacific, and an anomaly pattern over North America reminiscent of the Pacific-North American (PNA) or related Tropical/Northern Hemisphere (TNH) atmospheric teleconnections of ENSO; see Barnston and Livezey [1987]). This eigenvector exhibits a modest long-term negative trend, which, in the eastern tropical Pacific, describes a La Niña–like cooling trend (Cane et al. 1997) that opposes warming in the same region associated with the global warming pattern of the first eigenvector. This cooling trend has been punctuated recently, however, by a few large positive excursions (see Fig. 5) associated with the large El Niños of the 1980s and 1990s. The third eigenvector is associated largely with interannual- to decadal-scale variability in the Atlantic basin and carries the well-known temperature signature of the North Atlantic Oscillation and decadal tropical Atlantic variability (e.g., Chang et al. 1997). While there is no long-term trend in this pattern during the twentieth century, a recent decadal-scale upturn during the late 1980s to 1990s which has been noted elsewhere (see Hurrell 1995) is evident (Fig. 5). The fourth eigenvector describes a primarily multidecadal timescale variation with ENSO-scale and tropical/subtropical

Atlantic features. The fifth eigenvector is dominated by multidecadal variability in the entire Atlantic basin and neighboring regions that has been widely noted elsewhere (Folland et al. 1984; Delworth 1993, 1997; Kushnir 1994; Mann and Park 1994, 1996; Schlesinger and Ramankutty 1994; Mann et al. 1995; Delworth and Mann 1998). Eigenvectors #2 and #4 together describe more than 50% of the Niño-3 variance, and are the primary ENSO-related eigenvectors of the global temperature data, though additional ENSO-related variance is distributed among several lower-rank eigenvectors as well.

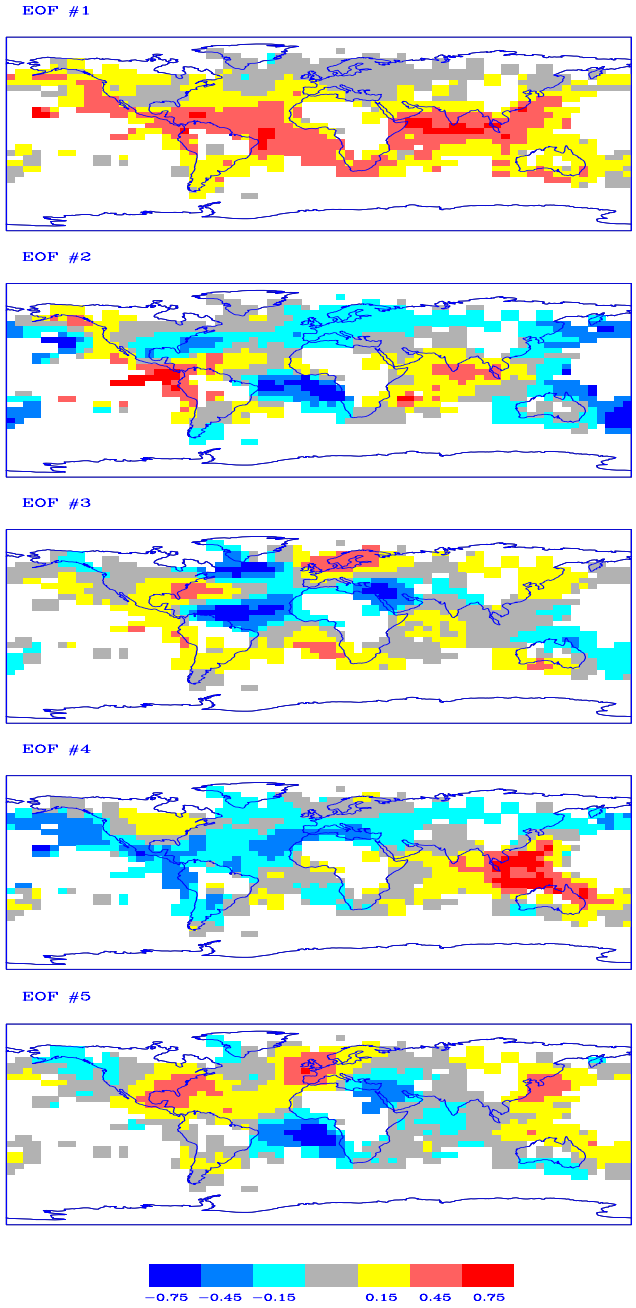

Fig. 4 Empirical orthogonal functions of the five leading eigenvectors of the 1902–93 global temperature data. The areal weighting factor used in the PCA (see text) has been removed, and the EOFs have been normalized by their maximum regional amplitude, so that relative spatial temperature variations can be inferred from the patterns shown.

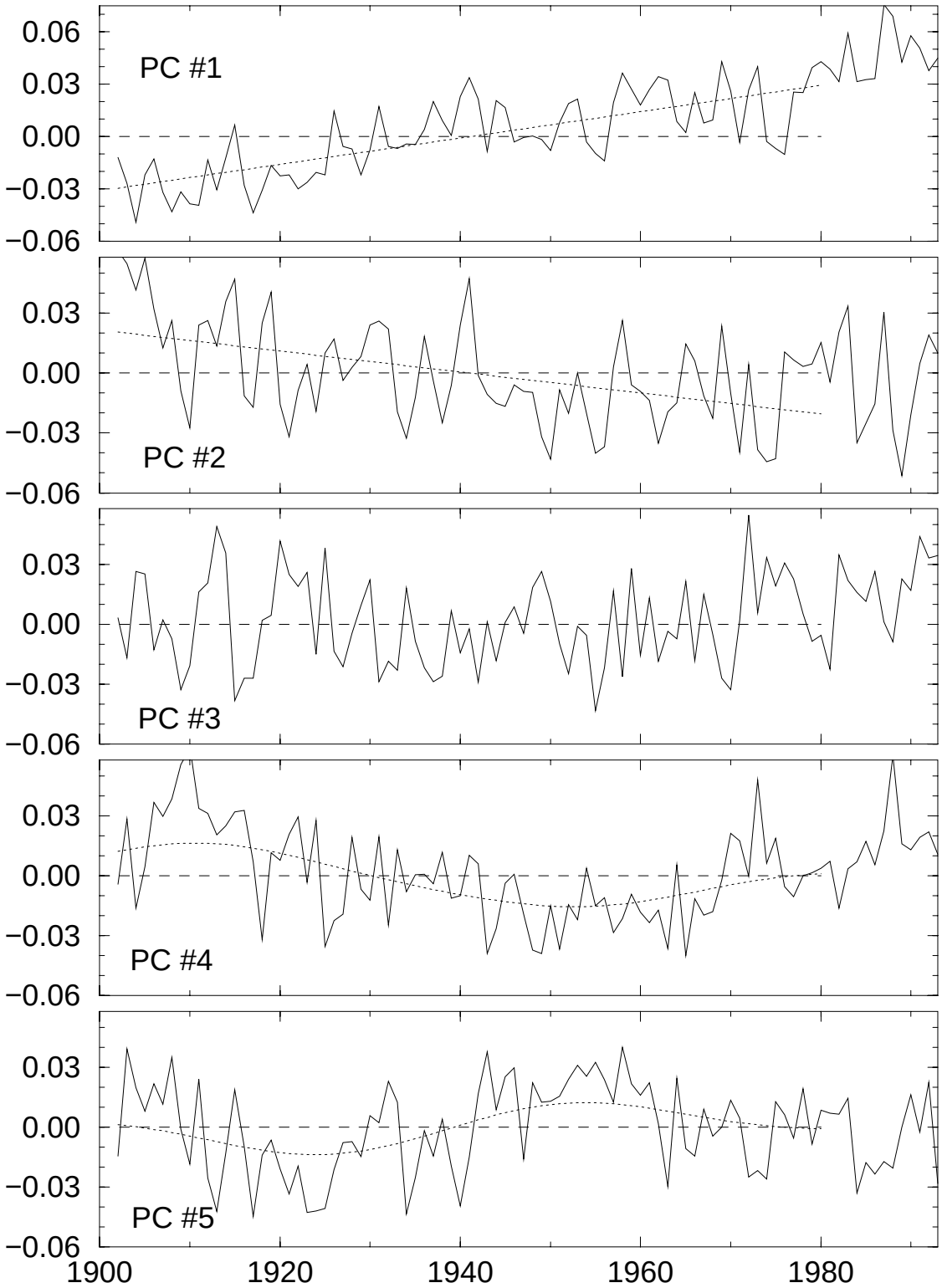

Fig. 5 Annual-mean PCs of the five leading eigenvectors of the 1902–93 global temperature data from 1902–93. The mean value (horizontal dashed lines) and any significant linear or multidecadal trends (dotted curves) for the individual PCs during the 1902–80 calibration period are also shown.

For the restricted tropical Pacific SST data set used for Niño-3 reconstruction, the first three eigenvectors turn out to be most important (see later), describing roughly equal shares of the 50% total resolved SST variance over the tropical Pacific region. While the spatial sampling is sparse in the region (see Fig. 3) it appears sufficient to describe much of the ENSO-related variability. The 3 eigenvectors describe a greater share of variance (b = 80%) in the Niño-3 index than do the first 20 global eigenvectors (74%; see Table 2). The EOFs are shown in Figure 6, while the associated PCs are shown in Figure 7. The second eigenvector carries much of the interannual variability associated with historical El Niño and La Niña events, while the first eigenvector describes the influence on the region of the globally synchronous warming pattern (i.e., global eigenvector #1) and the third eigenvector the offsetting negative trend in the eastern tropical Pacific (i.e., global eigenvector #2).

Table 2 Calibration and verification statistics for global reconstructions. Resolved variance statistics (β) are provided for the raw (1902–80) data (upper left corner), along with the squared correlation (r^2) of the raw Niño-3 series with the SOI series and its squared congruence statistic (g^2) with the historical QN92 El Niño chronology for reference. β statistics are also provided for the raw data after being filtered with the sets of eigenvectors used in the actual calibration experiments (upper right corner). For the calibration and verification experiments (lower table) the beginning year of the network employed ("NET") is given, along with the total number of (proxy and historical/instrumental) indicators ("$\#^T$"), number of historical/instrumental only indicators ("$\#^I$"), the total number and specific set of eigenvectors retained in calibration, calibration resolved variance β for global mean temperature (GLB), Northern Hemisphere mean temperature (NH), detrended Northern Hemisphere mean temperature (DET), Niño-3 index (NIN), and total spatial temperature field (MT), calibration squared correlation statistic of Niño-3 (NIN) with SOI series (r^2) and congruence statistic with QN92 chronology g^2. For verification, β statistics are given for GLB, NH, and MLT (the latter based on both [A] the 1854–1901 grid point data and the [B] 11 long instrumental temperature grid point records available; see text). Any positive value of β is statistically significant (see text) at greater than 95% (or for MULTb, 99%) while the statistical significance of the verification r^2 of Niño-3 with Southern Oscillation Index (SOI, 1865–1901) and squared congruence g^2 with the QN92 chronology (back through 1750) are explicitly denoted by the indicated symbols.

Raw Data (1902-08)						
β					r^{2a}	g^{2b}
GLB	NH	DET	NIN	MT	NIN	NIN
1.00	1.00	1.00	1.00	1.00	0.51	0.50

Eigenvector Filtering (1902-80)					
EVs	β				
	GLB	NH	DET	NIN	MT
1st 40	1.00	0.99	0.98	0.91	0.73
1st 20	0.99	0.99	0.97	0.74	0.58
1-5,9,11,14-16	0.95	0.93	0.87	0.72	0.40
1-5,9,11,15	0.95	0.93	0.78	0.70	0.38
1-3,6,8,11,15	0.92	0.83	0.69	0.65	0.31
1st 5	0.93	0.85	0.76	0.67	0.27
1,2,5,11,15	0.92	0.83	0.70	0.55	0.23
1,2,11,15	0.90	0.78	0.61	0.53	0.21
1,2	0.91	0.76	0.57	0.50	0.18
1	0.88	0.73	0.53	0.09	0.12

Table 2 (Continued)

				Calibration (1902-80)							Verification (pre-1902)					
Net	#T	#T		β					r^2	g^2	β				r^2	g^2
				GLB	NH	DET	NIN	MT	NIN	NIN	GLB	NH	MT[a]	MT[b]	NIN	NIN
1820	112	24	11 (1–5,7,9,11,14–16)	0.77	0.76	0.56	0.48	0.30	0.51	0.29	0.76	0.69	0.22	0.55	0.14**	0.28**
1800	102	15	"	0.76	0.75	0.54	0.50	0.27	0.52	0.30	0.75	0.68	0.19	0.45	0.10**	0.22**
1780	97	12	"	0.76	0.74	0.54	0.51	0.27	0.53	0.29	0.76	0.69	0.17	0.40	0.11**	0.20**
1760	93	8	9 (1–5,7,9,11,15)	0.76	0.74	0.52	0.49	0.26	0.52	0.29	0.75	0.70	0.17	0.33	0.10**	0.17*
1750	89	5	8 (1–3,5,6,8,11,15)	0.76	0.74	0.53	0.34	0.18	0.39	0.33	0.64	0.57	0.11	0.13	0.10**	0.19*
1730	79	3	5 (1,2,5,11,15)	0.74	0.71	0.47	0.23	0.15	0.30	0.29	0.65	0.61	0.11	0.13	0.05*	0.17*
1700	74	2	"	0.74	0.71	0.47	0.22	0.14	0.29	0.29	0.63	0.57	0.10	0.12	0.05*	0.15+
1650	57	1	4 (1,2,11,15)	0.72	0.67	0.42	0.05	0.14	0.19	0.23	0.61	0.53	0.12	0.10	0.02+	0.11*
1820[1]	88	0	8 (1–3,5,6,8,11,15)	0.76	0.73	0.51	0.31	0.19	0.37	0.31	0.65	0.56	0.11	0.19	0.12**	0.29*
1820[2]	24	24	2 (1,2)	0.32	0.28	-0.28	-0.27	0.10	0.07	0.20	0.30	0.37	0.11	0.26	0.0	0.16
1820[3]	42	24	7 (1–3,5,11,15,16)	0.50	0.50	0.13	0.05	0.17	0.22	0.18	0.56	0.53	0.17	0.47	0.09*	0.10
1750[3]	19	2	2 (1,2)	0.46	0.47	0.05	0.2	0.09	0.30	0.27	0.28	0.27	0.06	0.10	0.03+	0.15

+ (85% significant); * (90% significant); ** (95% significant); *** (99% significant); x (unphysical positive correlation obtained)

[a] (r^2 with SOI); [b] (g^2 w/QN92 chron)

[1] (no instrumental/historical data—proxy only; [2] (instrumental/historical data only); [3] (dendroclimatic indicators excluded)

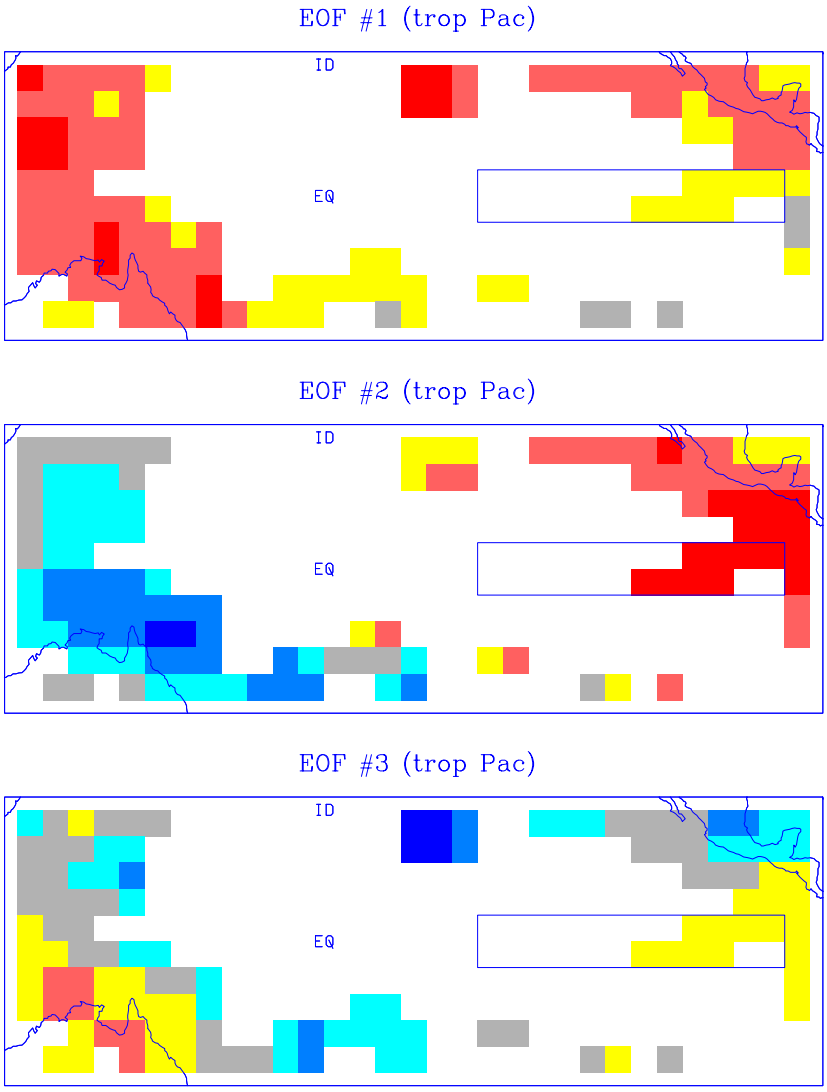

Fig. 6 Empirical orthogonal functions of the three leading eigenvectors of the 1902–93 restricted tropical Pacific region temperature data. Color-scale and other conventions are as in Figure 4.

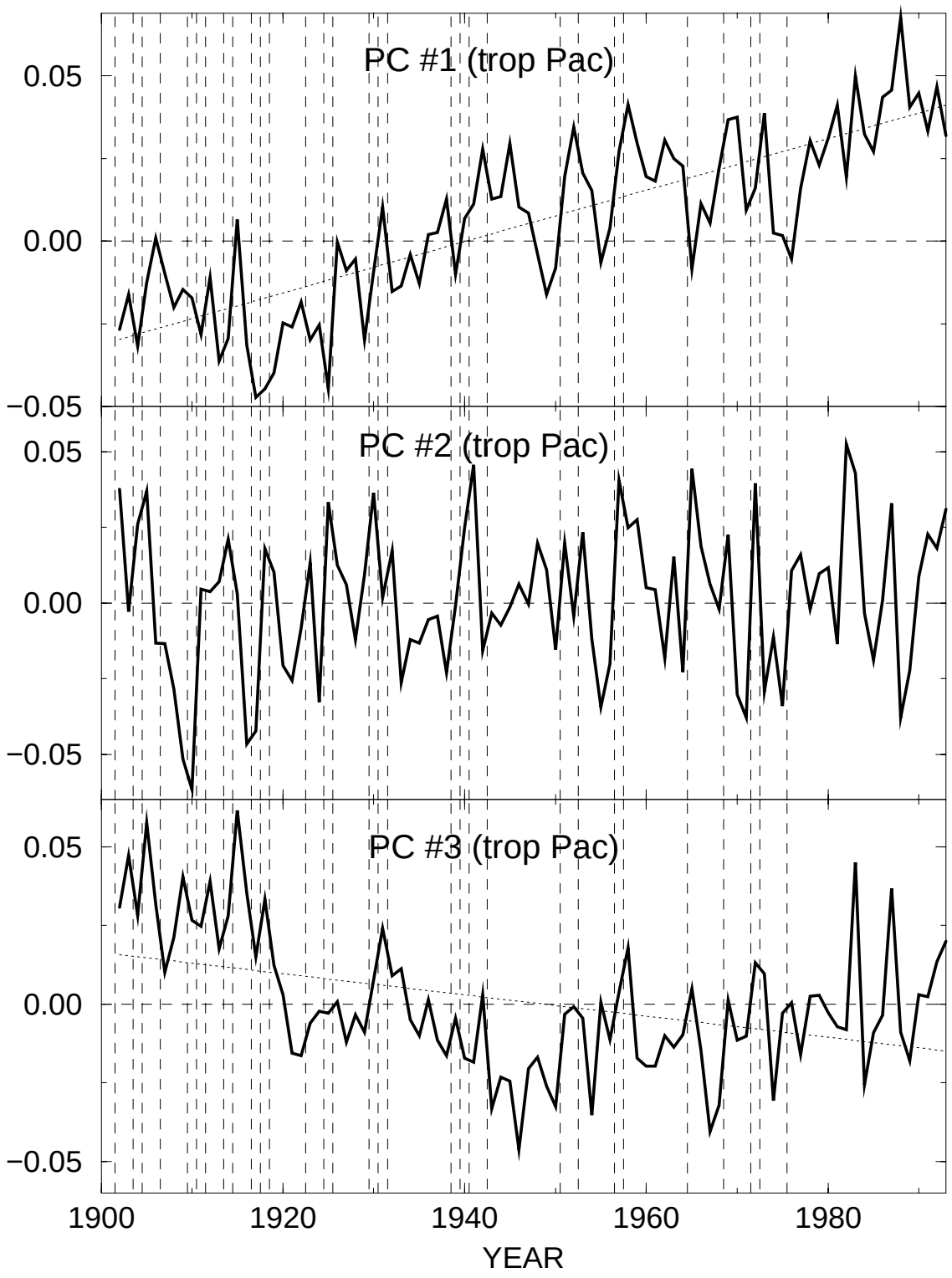

Fig. 7 Annual-mean PCs of the three leading eigenvectors of the 1902–93 restricted tropical Pacific region temperature data. Conventions are as in Figure 5. Vertical dashed lines indicate the timing of El Niño events as recorded in the QN92 chronology.

Having isolated the dominant spatiotemporal patterns of surface temperature variability in the instrumental record, we subsequently calibrate the multiproxy data networks against them at annual mean resolution. As described above, we seek to reconstruct only annual-mean conditions, exploiting the complementary information in data reflecting diverse seasonal windows of climate variability. The calibrations will provide a basis for reconstructing annual global patterns of temperature back in time from the multiproxy network, with a spatial coverage dictated by that available from the instrumental data the 1902–80 calibration period. In a given calibration exercise, we retain a specified subset of the annually averaged eigenvectors, the annually averaged PCs denoted by $\bar{u}_n^k$, where $n = 1,...,\bar{N}$, $\bar{N} = 79$ is the number of annual averages used of the N month length data set. In practice, only a small subset N_{eof} of the highest-rank eigenvectors turn out to be useful in these exercises from the standpoint of verifiable reconstructive skill. An objective criterion was used to determine the particular set of eigenvectors which should be used in the calibration as follows. Preisendorfer's (1988) selection rule, "rule N," was applied to the multiproxy network to determine the approximate number N_{eof} of significant independent climatic patterns that are resolved by the network, taking into account the approximate number of spatial degrees of freedom represented by the multiproxy data set. Because the ordering of various eigenvectors in terms of their prominence in the instrumental data, and their prominence as represented by the multiproxy network, need not be the same, we allowed for the selection of noncontiguous sequences of the instrumental eigenvectors. We used an objective criterion in which the group of N_{eof} of the highest-rank instrumental eigenvectors was chosen which optimized the calibration explained variance. Neither the measures of statistical skill nor the reconstructions themselves were highly sensitive to the precise criterion for selection, although it was considered encouraging from a self-consistency point of view that the objective criterion independently optimized, or nearly optimized, the verification explained verification statistics (discussed below).

These N_{eof} eigenvectors were trained against the N_{proxy} indicators, by finding the least-squares optimal combination of the N_{eof} PCs represented by each individual proxy indicator during the $\bar{N} = 79$ year training interval from 1902 to 1980 (the training interval is terminated at 1980 because many of the proxy series terminate at or shortly after 1980). The proxy series and PCs were formed into anomalies relative to the same 1902-08 reference period mean, and the proxy series were also normalized by their standard deviations during that period. This proxy-by-proxy calibration is well posed (i.e., a unique optimal solution exists) as long as $\bar{N} > N_{eof}$ (a limit never approached in this study) and can be expressed as the least-squares solution to the overdetermined matrix equation,

$$\underline{\mathbf{U}}\mathbf{x} = \mathbf{y}^{(\mathbf{p})}$$

$$\underline{\mathbf{U}} = \begin{bmatrix} \bar{u}_1^{(1)} & \bar{u}_1^{(2)} \ldots u_1^{(N_{eof})} \\ \bar{u}_2^{(1)} & \bar{u}_2^{(2)} \ldots u_2^{(N_{eof})} \\ & \ldots \\ \bar{u}_{\bar{N}}^{(1)} & \bar{u}_{\bar{N}}^{(2)} \ldots u_{\bar{N}}^{(N_{eof})} \end{bmatrix}$$

is the matrix of annual PCs, and

$$\mathbf{y}^{(\mathbf{p})} = \begin{bmatrix} y^{(p)}_1 \\ y^{(p)}_2 \\ \cdots \\ y^{(p)}_{\overline{N}} \end{bmatrix}$$

is the time series $\overline{N}$–vector for proxy record p.

The N_{eof}-length solution vector $\mathbf{x} = \mathbf{G^{(p)}}$ is obtained by solving the above overdetermined optimization problem by singular value decomposition (SVD) for each proxy record $p = 1, \ldots, P$. This yields a matrix of coefficients relating the different proxies to their closest linear combination of the N_{eof} PCs,

$$\underline{\mathbf{G}} = \begin{bmatrix} G_1^{(1)} & G_2^{(1)} \ldots G_{N_{eof}}^{(1)} \\ G_1^{(2)} & G_2^{(2)} \ldots G_{N_{eof}}^{(2)} \\ & \cdots \\ G_1^{(P)} & G_2^{(P)} \ldots G_{N_{eof}}^{(P)} \end{bmatrix}$$

This matrix of coefficients cannot simultaneously be satisfied in the regression, but rather represents a highly overdetermined relationship between the optimal weights on each of the N_{eof} PCs and the information in the multiproxy network at any given time.

Proxy-reconstructed patterns for the global temperature and tropical Pacific SST fields are finally obtained based on the year-by-year solution of the overdetermined matrix equation,

$$\underline{\mathbf{G}}\mathbf{z} = \mathbf{y}_{(j)}$$

where $y_{(j)}$ is the predictor vector of values of each of the P proxy indicators during year j. The predictand solution vector $\mathbf{z} = \hat{\mathbf{U}}$ contains the least-squares optimal values of each of the N_{eof} PCs for a given year.

This yearly reconstruction process leads to annual sequences of the optimal reconstructions of the retained PCs, which we term the reconstructed principal components, or RPCs, and denoted by $\boldsymbol{u^k}$. Once the RPCs are determined, the associated temperature patterns (of either the global field or tropical Pacific SST) are readily obtained through the appropriate eigenvector expansion,

$$\hat{\underline{\mathbf{T}}} = \sum_{k=1}^{N_{eof}} \lambda_k \hat{u}_k v_k$$

while quantities of interest (e.g., NH, Niño-3) are calculated from the appropriate spatial averages.

The optimization procedure described above to yield the RPCs is overdetermined (and thus well constrained) as long as $P > N_{eof}$, which is always realized in this study. An important feature

of our approach is that, unlike conventional transfer function approaches to paleoclimate reconstruction (see, e.g., Cook et al. 1994), there is no fixed relationship between a given proxy indicator (e.g., a particular coral or tree-ring series) and a given predictand (i.e., RPC) over the calibration interval. Instead, the best common choice of values for the small number of N_{eof} RPCs is determined from the mutual statistical information present in the network of multiproxy data on a year-by-year basis. The reconstruction approach is thus relatively resistant to errors or biases (e.g., dating errors) specific to any small number of indicators, in contrast to most conventional approaches.

To ensure the validity of the linear calibration procedure, we examined the calibration residuals, defined as the difference between the reconstructed and raw instrumental NH and Niño-3 series during the calibration interval (Fig. 8), for any evidence of bias. The distributions of the calibration residuals were found to be consistent with parent distributions of normal random deviates based on χ^2 tests applied to their respective histograms (NH significant at the 95% level; Niño-3 at the 99% level). These tests are shown graphically in Figure 9. The spectrum of the calibration residuals for these quantities, were, furthermore, found to be consistent with a "white" distribution showing little evidence for preferred or deficiently resolved timescales in the calibration process (see Mann et al. 1998b for a more detailed analysis). Having established unbiased calibration residuals, we were thus able to calculate uncertainties in the reconstructions from the uncalibrated calibration period variance. This uncalibrated variance increases back in time, as increasingly sparse multiproxy networks calibrate fewer numbers of eigenvectors back in time, and smaller fractions of instrumental variance (see Tables 2, 3). This decreased calibrated variance back in time is thus expressed in terms of uncertainties in the reconstructions which expand back in time. For the global temperature reconstructions back to 1650 of interest in the present study, the decreases in calibrated variance, and associated increases in uncertainties back in time, are quite modest (Table 2). For the Niño-3 reconstructions, they are negligible (Table 3).

Table 3 Calibration and verification statistics for tropical Pacific SST reconstructions, focusing on the diagnosed Niño-3 SST index. Resolved variance (β) statistics are provided for the raw (1902–80) Niño-3 index after being filtered with the sets of eigenvectors used in the actual calibration experiments, and the reconstructed/calibrated Niño-3 index. Other details are as described for Table 2.

Net	$\#^T$	$\#^T$	EVs	Calibration	Calibration	Verification	
					β (1902–80)	r^2(SOI, 1865–1901)	g^2(QN, 1750–1901)
1820	49	2	3 (1–3)	0.80	0.38	0.27***	0.39***
1800	45	0	”	”	0.42	0.22***	0.40***
1780	44	0	”	”	0.42	0.23***	0.38***
1750	43	0	”	”	0.42	0.23***	0.38***
1700	37	0	”	”	0.38	0.22***	0.38***
1650	29	0	”	”	0.34	0.20**	0.32*

*(95% significant)
**(99% significant)
***(99.5% significant

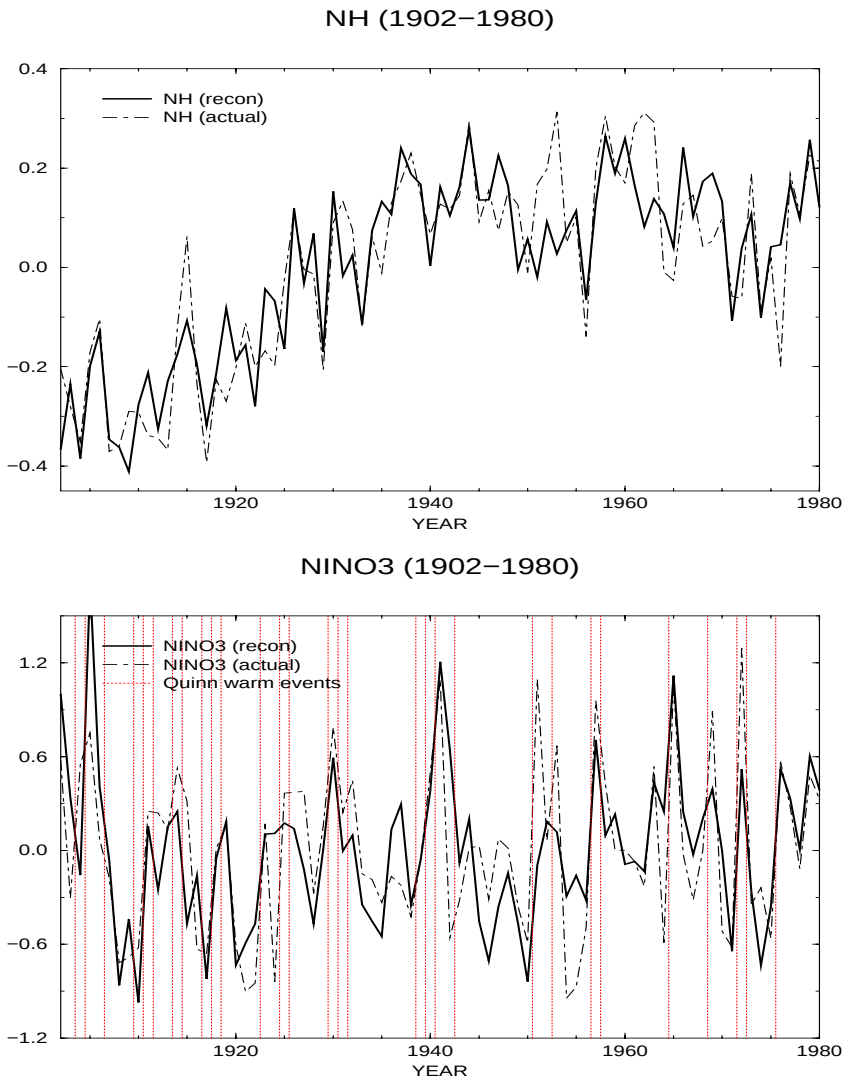

Fig. 8 Comparison of raw and reconstructed/calibrated (a) NH and (b) Niño-3 series during the 1902–80 calibration interval.

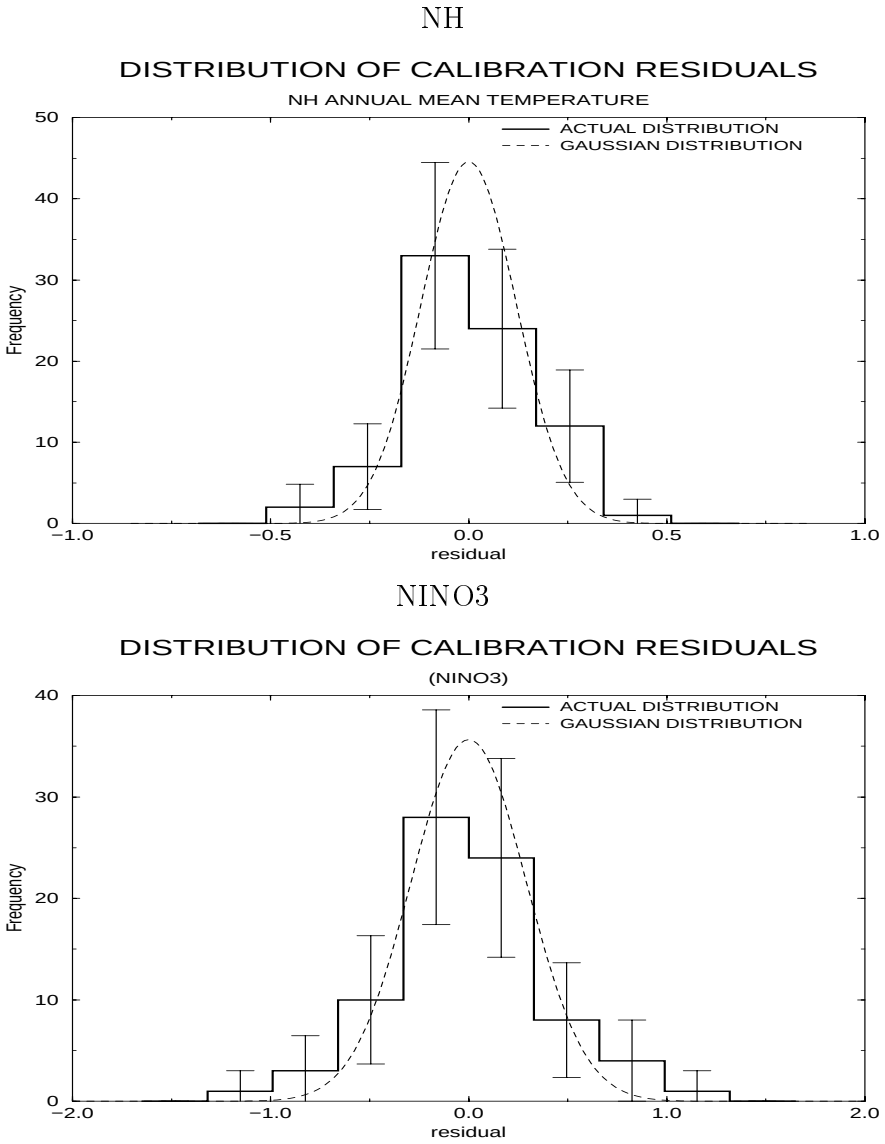

Fig. 9 Histogram of calibration residuals for (a) NH and (b) Niño-3 series. A Gaussian (normal) parent distribution is shown for comparison, along with 2 standard error bars for the frequencies of each bin. Both distributions are consistent with a Gaussian distribution at high levels of confidence (95% for NH, 99% for Niño-3).

Figure 10 compares the spectrum of the raw and reconstructed Niño-3 series during the calibration period (separately scaled so that their median power levels align). The calibrated series clearly captures the interannual band-limited features of the raw Niño-3 series. The calibrated series exhibits relatively more interdecadal-to-secular power, and relatively less quasibiennial power, than does the raw series. As was noted earlier, however, the spectrum of the calibration residuals (not shown) exhibits no statistically significant departure from the white spectrum expected for an unbiased reconstruction. It is particularly important that in the context of reconstructing low-frequency trends, there is no evidence of any loss of secular variance in calibration, and no reason to presuppose that multidecadal- to century-scale variations in ENSO are not adequately described in the reconstructions. Figure 11 compares the actual Niño-3 annual global temperature correlation pattern (that is, the pattern of the correlation coefficient of the

annual Niño-3 index with the annual global temperature field reconstructions) with the correlation pattern based on the multiproxy-reconstructed counterparts, for the 1902–80 calibration period. The multiproxy-based correlation pattern clearly captures the details of the observed correlation pattern during the calibration period, giving some justification to analyzing changing correlation patterns back in time from the reconstructions.

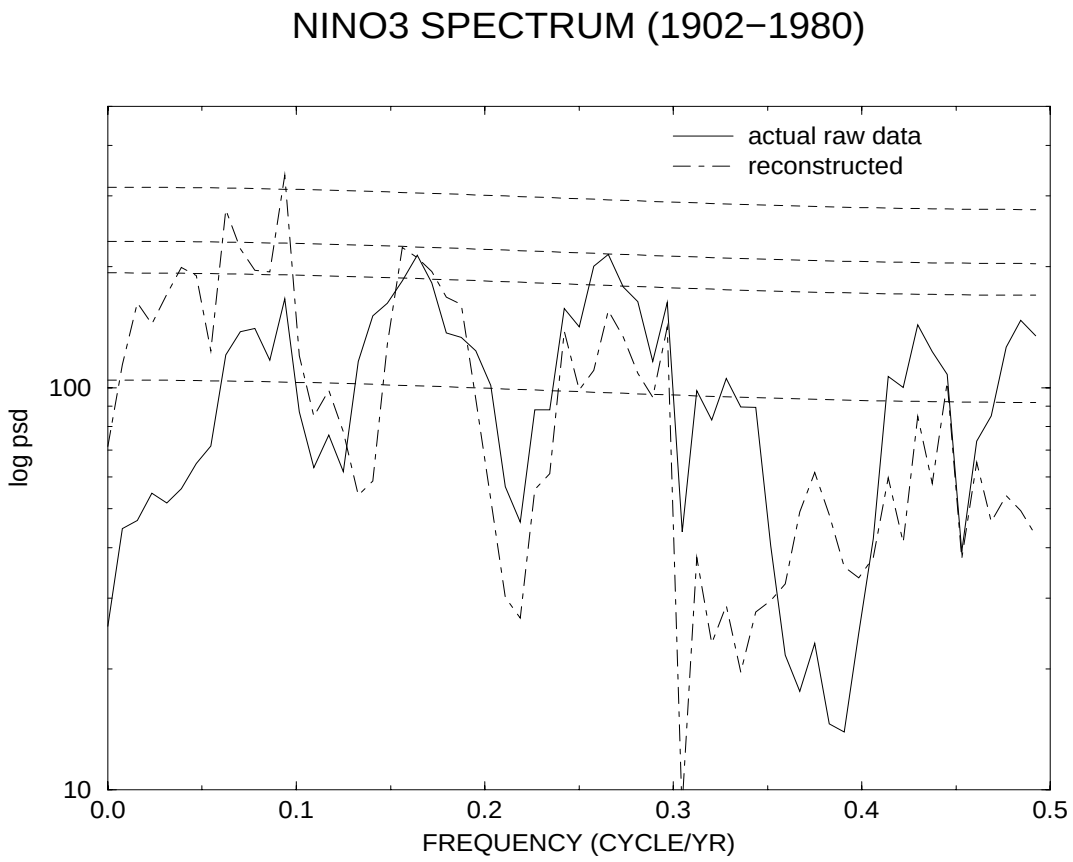

Fig. 10 Spectrum of raw instrumental (solid) and reconstructed/calibrated (dashed) Niño-3 series during the 1902–80 calibration period. The spectrum is calculated by using the multitaper method (Thomson 1982; Park et al. 1987; Mann and Lees 1996) based on three tapers and a time-frequency bandwidth product of $W = 2N$.

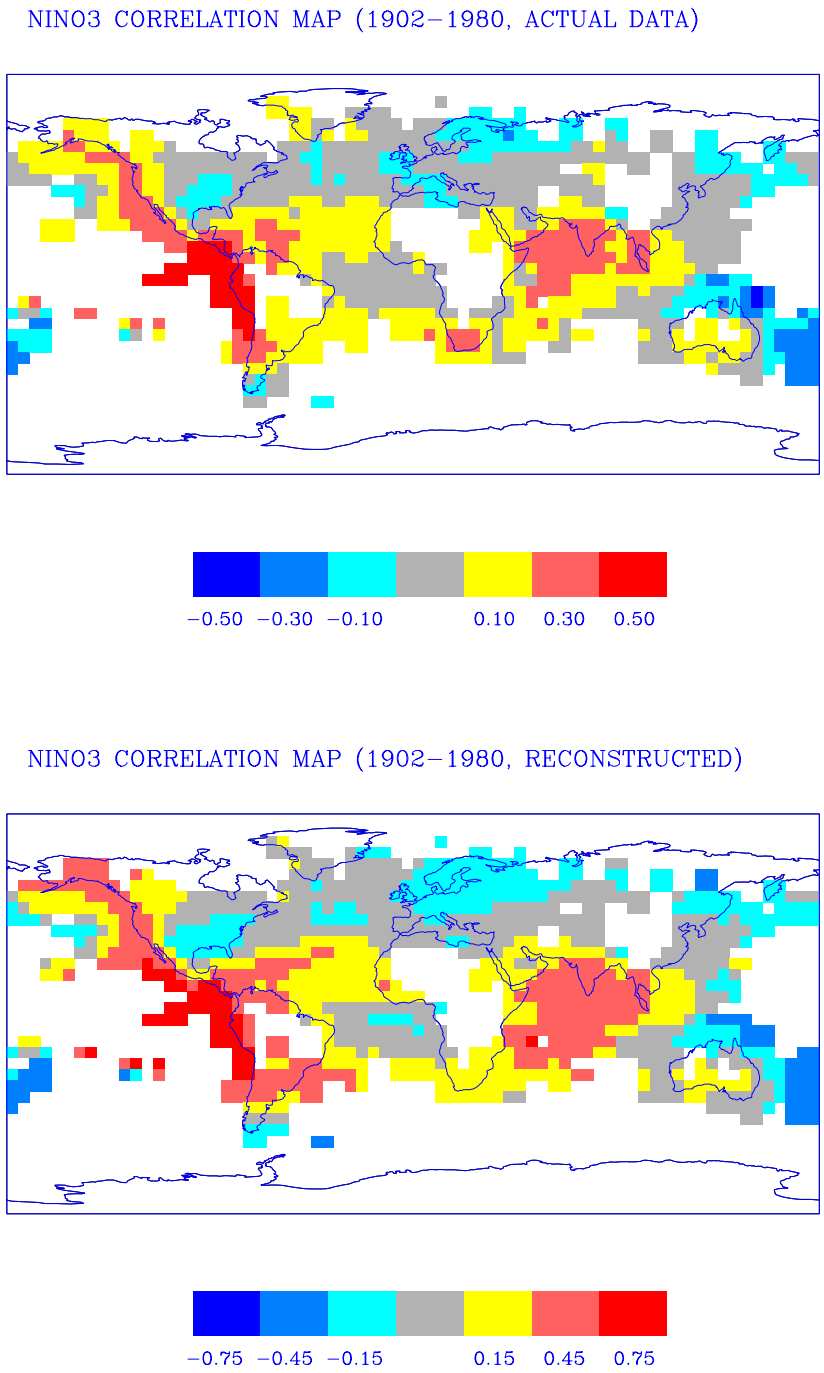

Fig. 11 Niño-3 correlation map during1902–80 calibration period based on (top) raw data and (bottom) reconstructed/ calibrated Niño-3 and global temperature patterns. The color scale indicates the specific level of correlation with a given grid point, with any color value outside of gray significant at greater than roughly the 80% level based on a two-sided test. Red and blue indicated significance well above the ~99% confidence level.

The skill of the temperature reconstructions (i.e., their statistical validity) is independently established through a variety of complementary independent cross-validation or “verification” exercises. The numerical results of the calibration and verification experiments are summarized in

Table 2 for the global pattern reconstructions and in Table 3 for the Pacific SST reconstructions upon which the Niño-3 index is ultimately based. Four distinct sources of verification were used for the global reconstructions: (1) widespread instrumental grid point data ($M' = 219$ grid points; see Fig. 3) available for the period 1854–1901, (2) a small subset of 11 very long estimated instrumental temperature grid point averages (10 in Eurasia, 1 in North America; see Fig. 1) constructed from the longest available station measurement (each of these "grid point" series shared at least 70% of their variance with the corresponding temperature grid point available during 1854–1980, providing verification back to at least 1820 in all cases (and back through the mid- and early eighteenth century in many cases), (3) the SOI available for corroboration of ENSO-scale variability during the late nineteenth century, and (4) the QN92 historical chronology of El Niño events dating back into the sixteenth century. Exercise (1) provides the only means of widespread instrumental spatial verification, but only experiment (3) provides instrumental verification of the Niño-3 region, while exercises (2) and (4) address the fidelity of long-term variability. Only verification experiments (3) and (4) were used to diagnose (in terms of the Niño-3 index) the quality of the tropical Pacific pattern reconstructions. Note (compare Tables 2 and 3) that the calibration and verification experiments indicate a more skillful Niño-3 index from the tropical Pacific SST-based reconstructions than from the global reconstructions.

The spatial patterns of described variance (β) for both calibration (based on 1902–80 data) and verification (based on verification experiments [1] consisting of the withheld instrumental grid point data for 1854–1901) are shown for the global reconstructions in Figure 12. Experiments [2] provide a longer-term, albeit an even less spatially representative, multivariate verification statistic ("MULTb"). In this case, the spatial sampling does not permit meaningful estimates of NH or GLB mean quantities. In any of these diagnostics, a positive value of β is statistically significant at greater than 99% confidence as established from Monte Carlo simulations. Verification skills for the Niño-3 reconstructions were estimated indirectly by experiments [3] and [4], since a reliable instrumental Niño-3 index was not available far beyond the beginning of the calibration period. The (negative) correlation r of Niño-3 with the SOI annual mean for 1865–1901 (obtained from P.D. Jones, personal communication) and a squared congruence statistic g^2 measuring the categorical match between the distribution of warm Niño-3 events and the distribution of warm episodes according to the QN92 historical chronology (available back through 1525) were used for statistical cross-validation of the Niño-3 index, with significance levels estimated from standard one-sided tables and Monte Carlo simulations, respectively. The verification period comparisons are shown in Figure 13. The r^2 of the Niño-3 index with this instrumental SOI is a lower bound on a true Niño-3 verification b, since the shared variance between the instrumental annual mean Niño-3 and SOI indices, as commented upon earlier, is itself only ≈50% (see Table 2). Thus, it is possible that a $r^2 = 0.25$ might be tantamount to a true verification described variance score of $\beta \approx 0.5$, and the verification r^2 scores should be interpreted in this context. The calibration and verification experiments thus suggest that we skillfully describe about 70–80% of the true NH variance back to 1820 (see Table 2), and about 38–42% of the true Niño-3 variance in the optimal index back to 1700 (see Table 3). Scores for earlier reconstructions are slightly lower in each case (see Tables 2 and 3). We note that the verifiable statistical skill in our annual-mean Niño-3 index is similar to that of the best independent recent ENSO reconstructions. For example, Stahle et al. (1998) reconstruct a winter SOI back to 1706, indicating 53% resolved instrumental variance for a more restricted December–February season. Multidecadal and longer-term trends of interest here, however, were not resolved in that study. In addition to the above means of cross-validation, we also tested the network for sensitivity to the inclusion or elimination of particular trainee data (e.g.,

instrumental records, the northern tree line dendroclimatic indicators of North America, and tropical coral records). These sensitivity experiments are also described (for the global pattern reconstructions) in Table 2.

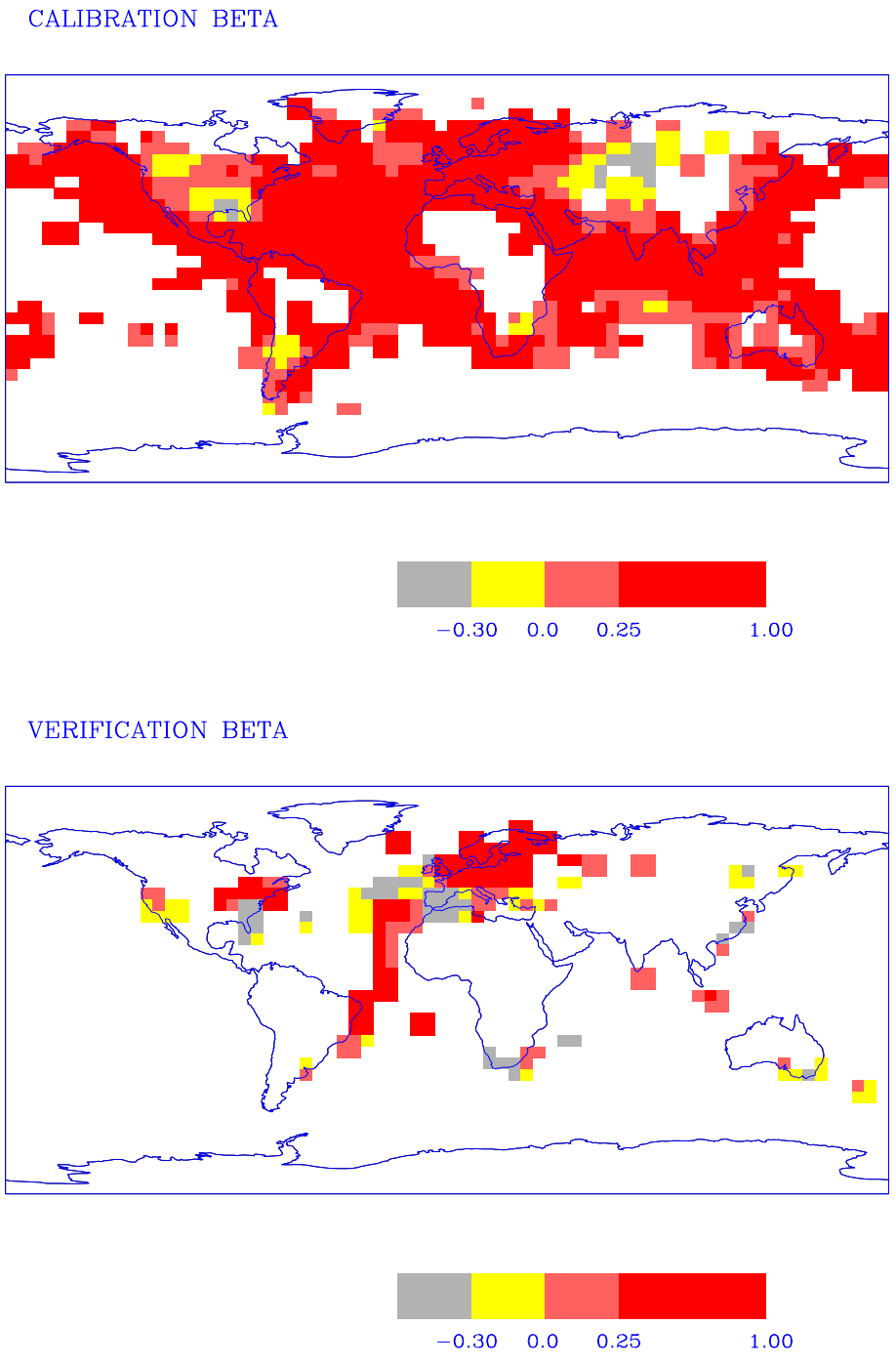

Fig. 12 Pattern of calibration (top, based on 1902–80 data) and verification (bottom, based on 1854–1901 "withheld" data) resolved variance statistic β for the global reconstructions. Values that are insignificant at the 99% level are shown in gray, while negative, but 99% significant values are shown in yellow, and significant positive values are shown in two shades of red. The significance estimation procedure is described in the text.

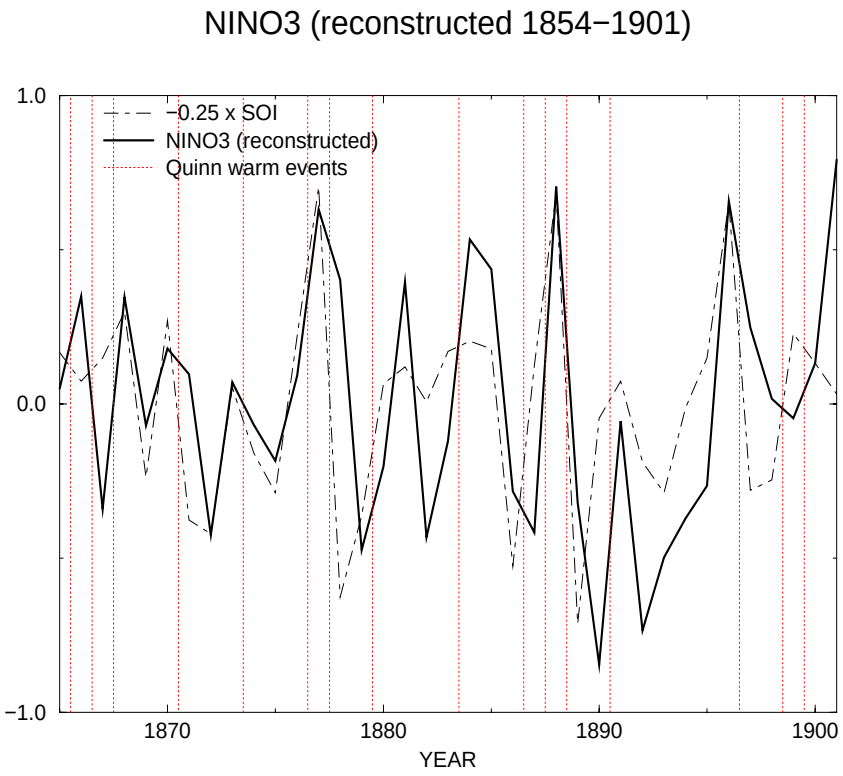

Fig. 13 Reconstructed Niño-3 series along with the (negative and rescaled) SOI series (dot-dashed) during the 1865–1901 sub-interval of the pre-calibration "verification" period during which the SOI is available. The timing of El Niño events as recorded in the QN92 chronology is shown for comparison.

To illustrate the effectiveness of the proxy pattern reconstruction procedure, we show as an example (Fig. 14) the raw, EOF-filtered, and reconstructed temperature patterns for a year during the calibration interval (1941) for which the true large-scale surface temperature pattern is known. The reconstructed pattern is a good approximation to the smoothed anomaly pattern obtained by filtering the raw data by the same 11 eigenvectors used in the calibration process (retaining about 40% of the total spatial variance). The historically documented El Niño and associated Pacific/ North American temperature anomalies are clearly captured in the reconstruction, as are the prominent cold anomalies in Eurasia. This example serves to demonstrate the level of resolved spatial variance that can typically be expected in the pre-instrumental reconstructed global temperature patterns discussed below.

Temperature reconstructions

We analyze the reconstructions of global temperature patterns and the Niño-3 index back to 1650. Temperature pattern reconstructions back to 1400 are discussed elsewhere (MBH98; Mann et al. 1998b); here, we choose to focus on the past four centuries, for which the global ENSO phenomenon can be most skillfully reconstructed. The reconstructed global temperature patterns are derived by using the optimal eigenvector subsets determined in the global calibration experiments (see Table 2, 11 eigenvectors for 1780–1980, 9 eigenvectors for 1760–79, 8

eigenvectors for 1750–59, 5 eigenvectors for 1700–49, 4 eigenvectors for 1650–99), while the Niño-3 index is based on the tropical Pacific SST reconstructions for which the optimal eigenvector subset includes the first 3 eigenvectors for the period 1650–1980 (see Table 3).

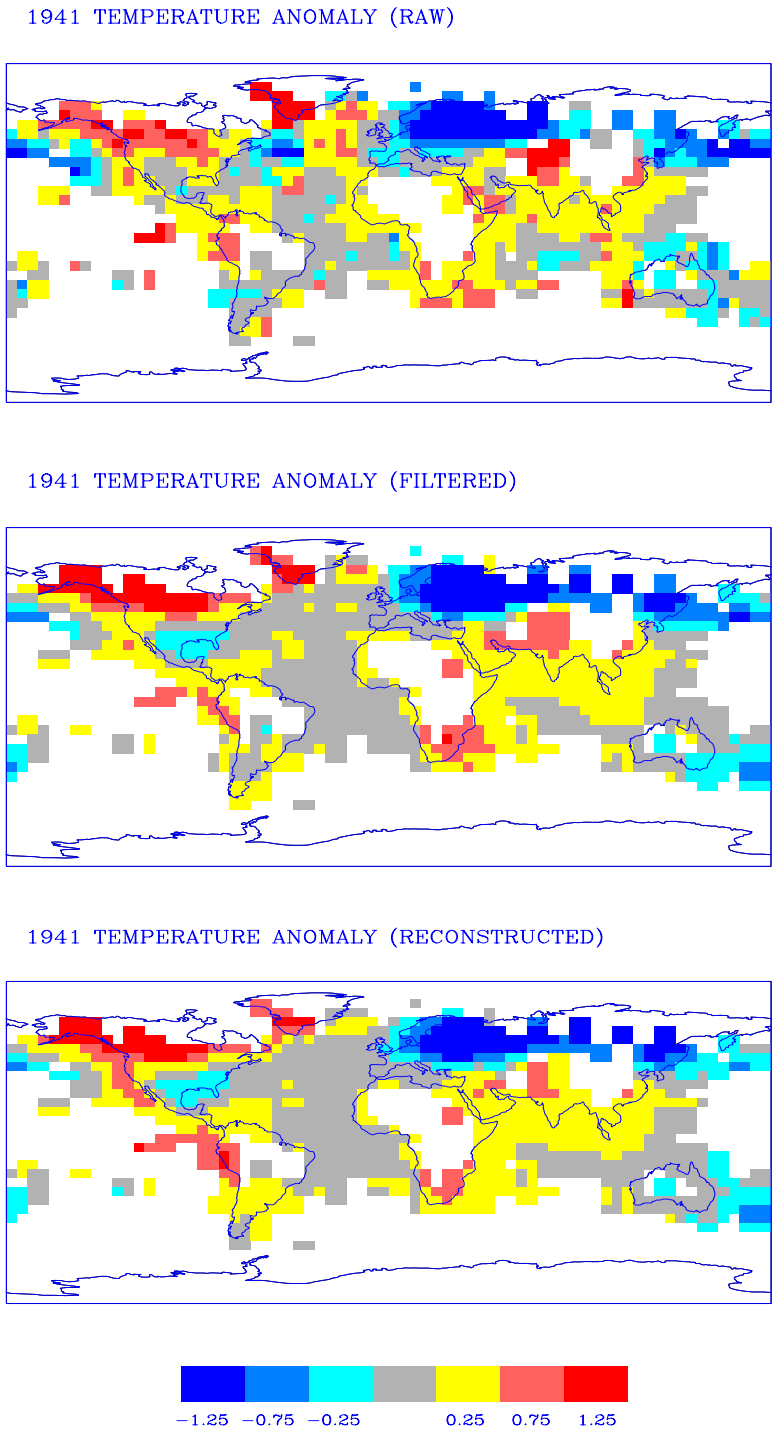

Fig. 14 Comparison of the proxy-reconstructed temperature anomaly pattern for 1941 with raw data, showing (top) actual, middle (EOF-filtered), and (bottom) reconstructed/calibrated pattern. Anomalies are indicated by the color scale shown, relative to the 1902–80 climatology.

Large-scale trends

It is interesting to consider the temporal variations in the first five global RPCs (Fig. 15), associated with the estimated variations in the different spatial patterns (EOFs) shown in Figure 4 prior to the twentieth century (see MBH98). The positive trend in RPC #1 during the twentieth century is clearly exceptional in the context of the long-term variability in the associated eigenvector, and indeed describes much of the unprecedented warming of the twentieth century as was discussed earlier. Reconstructed principal components #2 and #4 are associated with the primary ENSO-related eigenvectors in the global data set, and serve to describe much of the long-term variation in the global ENSO phenomenon expressed in the global pattern reconstructions. The negative trend in RPC #2 during the past century (see earlier discussion), which is anomalous in the context of the longer-term evolution of the associated eigenvector, is particularly interesting in the context of ENSO-scale variations. This recent negative trend, describing a cooling in the eastern tropical Pacific superimposed on the warming trend in the same region associated with the pattern of eigenvector #1, could plausibly be a modulating negative feedback on global warming (Cane et al. 1997). Reconstructed PC #4, associated with a more modest share of ENSO-related variability, shows a pronounced multidecadal variation, though no obvious linear trend, during the twentieth century, but more muted variability prior to the twentieth century. Reconstructed PC #5 exhibits notable multidecadal variability throughout the modern and pre-calibration periods, associated with the wavelike trend of warming and subsequent cooling of the North Atlantic this century discussed earlier, and the robust multidecadal oscillations in that region detected in a previous analysis of multiproxy data networks (Mann et al. 1995). This variability may be associated with ocean-atmosphere processes related to the North Atlantic thermohaline circulation (Delworth et al. 1993, 1997) and is further discussed by Delworth and Mann (1998).

Tropical Pacific and Niño-3 variations

In Figure 16, we show the three RPCs corresponding to the separate tropical Pacific reconstructions. As in the calibration interval (see Fig. 7), the interannual ENSO-related variability remains dominated by the RPC #2, while RPCs #1 and #3 describe in large part the anomalous trends during the twentieth century in the region discussed earlier. The reconstructed Niño-3 index (Fig. 17) places recent large ENSO events in the context of a several centuries–long record, allowing us to better gauge how unusual recent behavior might be. Indeed, the anomalous 1982/1983 El Niño event represents the largest positive event in our reconstructed chronology back to 1650. A similar statement holds for the current 1997/1998 event (not shown in Fig. 17), which is of similar magnitude. Taking into account the uncertainties in the pre–twentieth-century reconstructions, however, a more guarded statement is warranted. The 1982/1983 and 1997/1998 events are both slightly greater than 2 standard errors (2s) warmer than any reconstructed, pre-1902 event. However, there are nine reconstructed events that are within 1.5-2.0 standard errors of either of these two events. Roughly speaking, this lowers the probability to about 80% that either of the two events in question is warmer than *any other single event* back to 1650, taking into account the current uncertainties in the reconstruction. The significance of the occurrence of two such *reasonably* unlikely events in the past 16 years, however, should clearly not be dismissed. Possible indications of a recent change in the state of El Niño are discussed further in later sections.

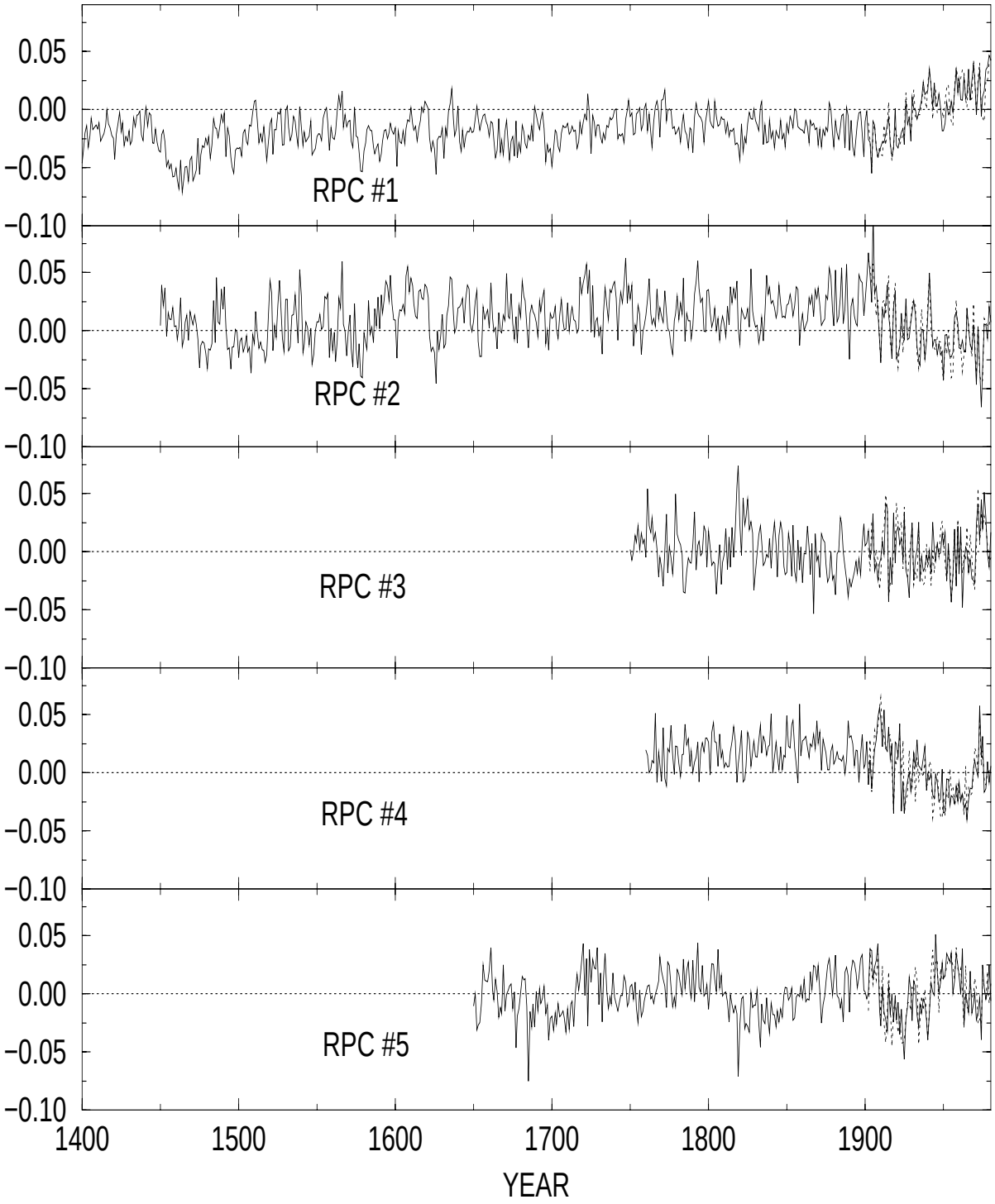

Fig. 15 Time reconstructions (RPCs-solid) and 1902–93 raw data (PCs-dotted) for the first five global eigenvectors. 1902–80 calibration period means are indicated by the horizontal dotted lines.

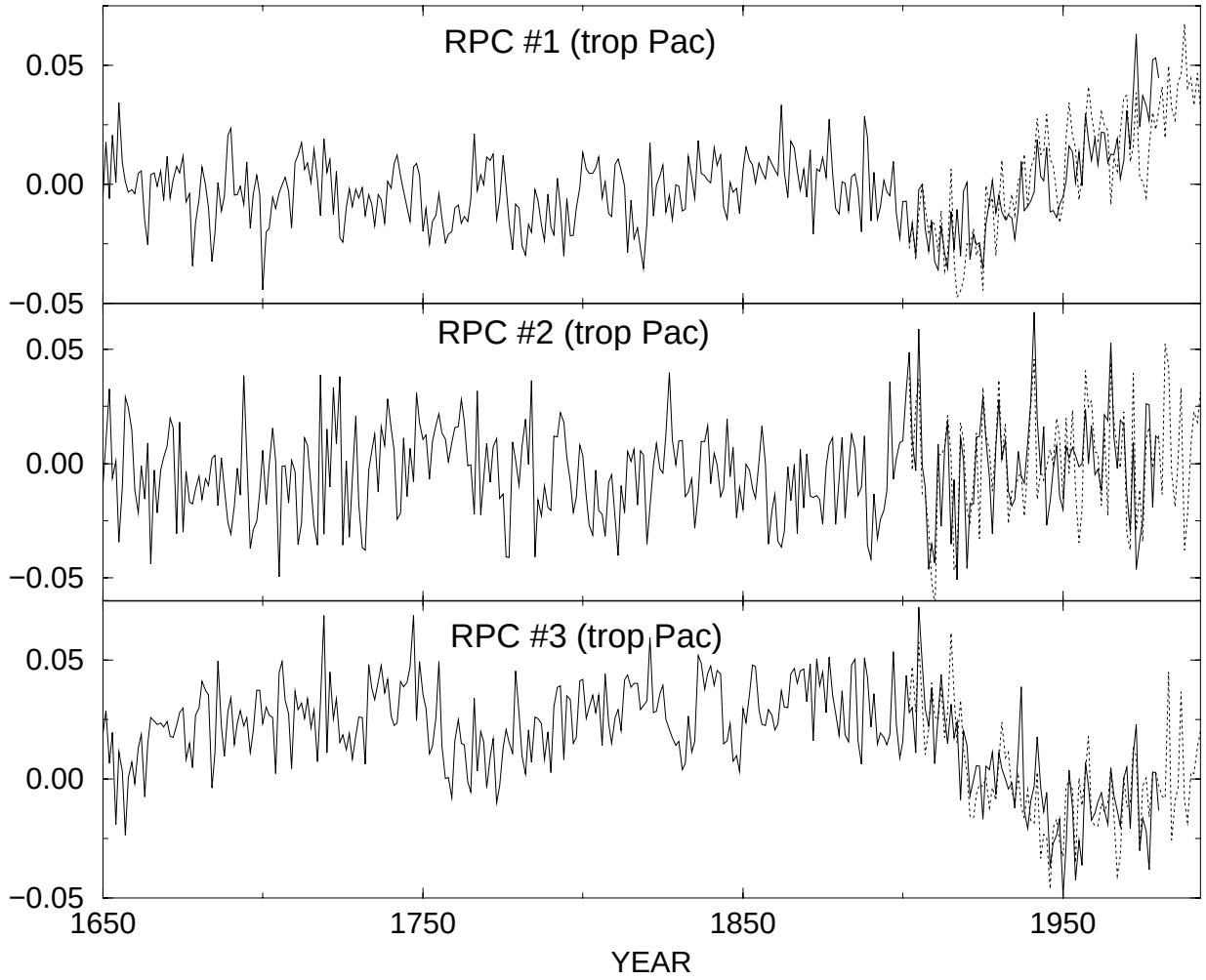

Fig. 16 Time reconstructions (RPCs-solid) and 1902–93 raw data (PCs-dotted) for the three eigenvectors of the restricted tropical Pacific temperature data.

ENSO and global influences

Details of the NH mean annual temperature series and associated implications for natural and anthropogenic forcing of global climate during past centuries are discussed by MBH98. Here, we use the NH series to focus on relationships between hemispheric to global-scale temperature variation, and the ENSO-scale variations captured in the separately determined Niño-3 reconstruction. We seek in particular to understand how changes in ENSO, themselves either internally or externally forced in nature, may have influenced global or hemispheric temperature trends over time. Due primarily to the poleward transport of anomalous tropical Pacific heat, warm ENSO events (i.e., El Niños) are typically associated with warm hemispheric or global conditions, while cold ENSO events (i.e., La Niñas) are typically associated with cold conditions (typically on the order of positive and negative 0.1°C for the globe, respectively; see, e.g., Jones 1989; Angell 1990). Thus, it is not unreasonable to suppose that changes in ENSO could lead to modest changes in global and hemispheric temperatures. The relationship between the reconstructed NH and Niño-3 series is shown in Figure 18 (the Niño-3 index is scaled by a factor of 0.25 so that a typical ENSO

event—e.g., a 0.5°C Niño-3 anomaly—is roughly in scale with an expected ~0.1°C NH mean temperature anomaly). Overall, the two series are modestly correlated (r = 0.14 for the 244-year period 1650–1993, compared), which is significant at well above the 99% level whether or not a one-sided or two-sided significance test is used (one could argue that only a positive correlation should be sought on physical grounds). However, the implied shared variance between the two series is less than 2%, which suggests that ENSO is not a dominant influence on changes in hemispheric or global mean temperatures, at least in comparison with external forcing agents (see MBH98). Both Niño-3 and NH do show similar low-frequency variations at times, however (compare the 50-year smoothed curves in Fig. 18), with warming occurring in both cases during the seventeenth/early eighteenth, and twentieth centuries. The low-frequency variations in Niño-3 are nonetheless relatively muted compared to those in NH, particularly during the twentieth century, when NH warming appears to become dominated by greenhouse forcing (IPCC 1995; MBH98). In contrast to the NH series, there is no evidence of any significant long-term departures from the twentieth-century climatology (see Fig. 17). There are in fact notable periods during which the low-frequency trends are uncorrelated or even opposite (e.g., late eighteenth century through mid-nineteenth century). It is interesting, though perhaps coincidental, that this latter period corresponds to an anomalously cool period for the Northern Hemisphere on the whole, associated with low solar irradiance, and preceding any greenhouse warming (see MBH98, Fig. 7). As is discussed in later sections, this is also a period of anomalously weak amplitude interannual variability in ENSO, and unusual global patterns of ENSO temperature influence.

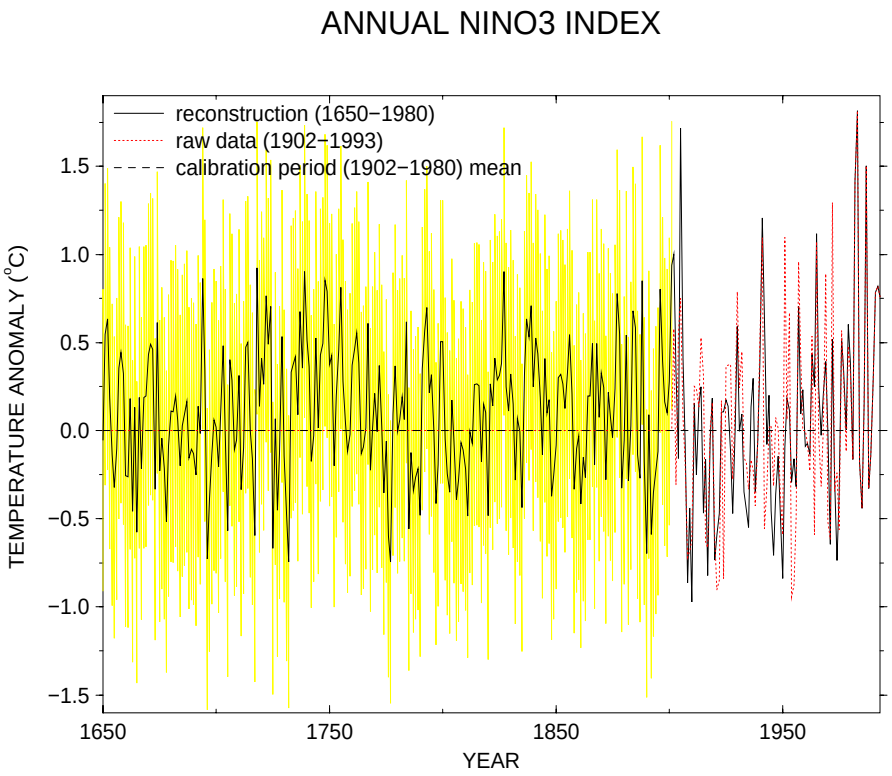

Fig. 17 Reconstructed Niño-3 index back to 1650, along with instrumental series from 1902–93. The region contained by the positive and negative 2 standard uncertainty limits in the reconstruction is shown (shaded) prior to the instrumental calibration period. The calibration period (1902–80) mean is shown by the horizontal dashed line.

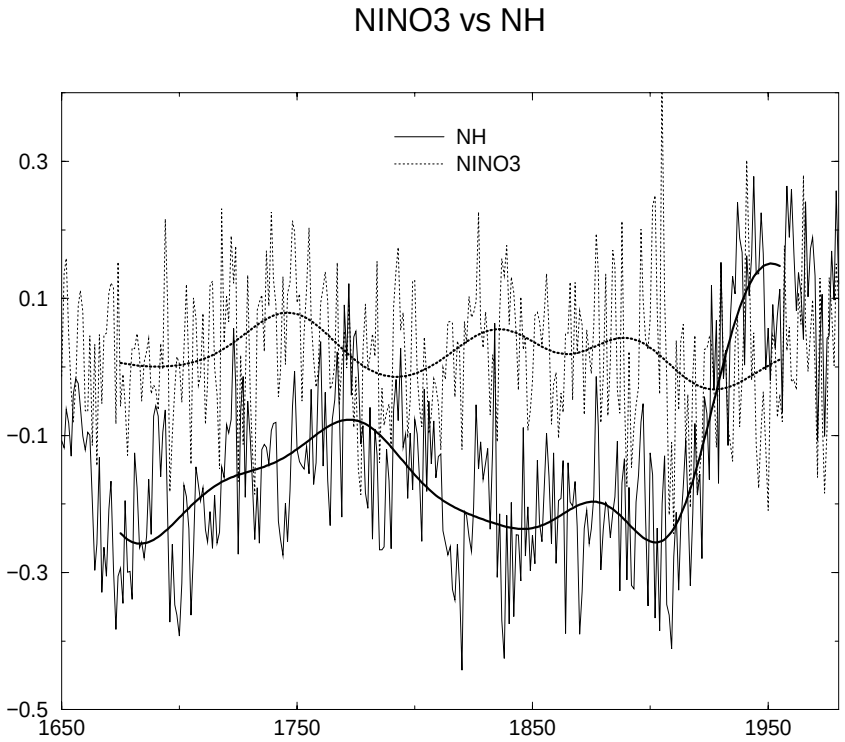

Fig. 18 Comparison of reconstructed Northern Hemisphere (NH) mean annual temperature series and Niño-3 index (rescaled by a factor of 0.25) from 1650–1980, along with 50-year smoothed versions of each series.

The muted positive trend in Niño-3 relative to that in NH during the twentieth century can be attributed to the negative twentieth-century trend in eigenvector #2 noted earlier. As was also discussed earlier, this offsetting trend might in turn be related to the negative feedback to greenhouse warming discussed by Cane et al. (1997). On the other hand, there is a strong apparent relationship between global temperature increases and warm ENSO conditions during the more brief period of the past couple decades (e.g., Trenberth 1990), and this period coincides with what appear to be the warmest hemispheric conditions of the past six centuries (MBH98). There is, furthermore, evidence of distinct and unusual dynamical behavior of ENSO during this most recent period. For example, Goddard and Graham (1998) argue for a breakdown of the classical delayed oscillator mechanism in describing the vertical oceanographic evolution of ENSO-like variations during the 1990s. Interdecadal ENSO-like variability (as discussed below) complicates any simple interpretation of trends in ENSO during the most recent decades, however. Thus, while the long-term relationships between ENSO and global temperature changes appear modest based on our reconstructions, the possible relationships between recent global warming and changes in ENSO are not yet clearly resolved.

Stationarity of ENSO teleconnections

It is also of interest to estimate the changes over time in the global pattern of influence of ENSO (i.e., the "teleconnections" of ENSO). Figure 11 showed that the modern global ENSO pattern—as described through the global correlation map of the Niño-3 index—is well captured by our multiproxy calibrations. Though the global patterns of ENSO in our reconstructions are

described by a limited number of distinct global patterns or degrees of freedom, and not all features are expected to be well described given the variable spatial reconstructive skill of the global reconstructions (e.g., parts of the southeastern United States; see Fig. 12). However, while the details of different ENSO events may be described only approximately, it is certainly true that different "flavors" of the global ENSO phenomenon are reasonably well described. This is evident in the reconstructions of global temperature patterns for specific ENSO years shown in a later section.

We examine how the global ENSO pattern changes over time by evaluating the correlation map of the reconstructed Niño-3 index against the global temperature pattern reconstructions in successive 50-year periods back to 1650 (Fig. 19). Certain features of the pattern appear remarkably robust, while other features are more variable. In all cases, the classic "horseshoe" pattern of a warm eastern tropical Pacific and west coast of North America, and a cold central North Pacific, is observed. This pattern might be regarded as an extremely robust signature of ENSO, at least over multidecadal and longer periods of time, while teleconnections into North America, and especially the Atlantic, and Eurasia are clearly more variable (the reader should keep in mind that the weaker features of these correlation maps are only marginally significant). The considerable variability between different 50-year periods in the North American teleconnection is consistent with the observations of Cole and Cook (1997) of multidecadal changes in ENSO-related patterns of drought in North America. The most striking evidence of a non-stationarity in ENSO teleconnections is the departure of the pattern of 1801–50 from the pattern dominated by all other periods. In particular, the pattern for this period shows a distinct absence of the typical pattern of warming in the far western tropical Pacific, an expanded region of cooling over eastern and southern North America, and cooling, rather than the typical warming, in the western equatorial Atlantic, coinciding with warm-event conditions. We believe that this pattern arises from a breakdown of interannual band ENSO variability during this period that may be related to external forcing of the global climate (see below). In the absence of the more typical interannual pattern, a somewhat different decadal-scale ENSO-like pattern of variability, which appears more robust over time, dominates during this period. It is through this suppression of the typical interannual pattern of variability, that external forcing may lead to changes in extratropical ENSO teleconnections (see, e.g., the modeling study of Meehl and Branstator 1992 of the response to doubled CO_2; unfortunately, changes in the frequency domain characteristics of ENSO were not addressed in that study). The distinction between patterns of interannual and decadal ENSO variability has been discussed elsewhere (e.g., Trenberth and Hurrell 1994; Graham 1994; Mann and Park 1994, 1996; Knutson et al. 1997; Goddard and Graham 1998).

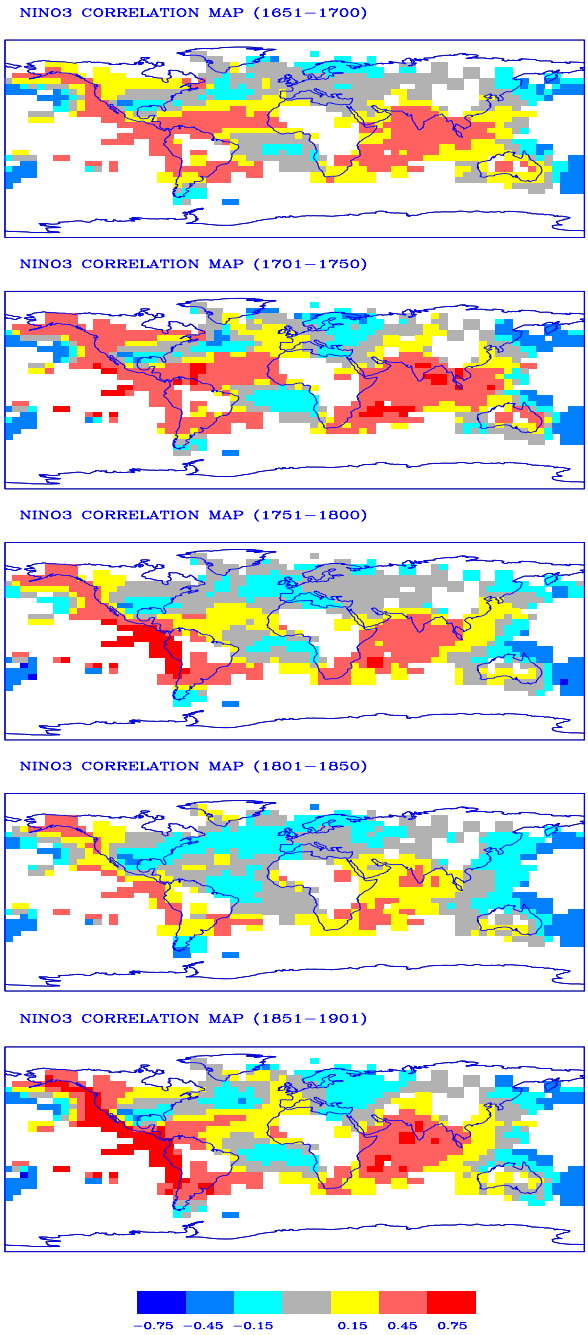

Fig. 19 Niño-3 temperature correlation map in successive 50-year periods between 1650 and present. The color scale shown indicates the specific level of correlation with a given grid point, with any color value outside of the gray category indicating significance at greater than a 70% level (based on a two-sided test), and with blue and red indicating significance at well above the 99% level.

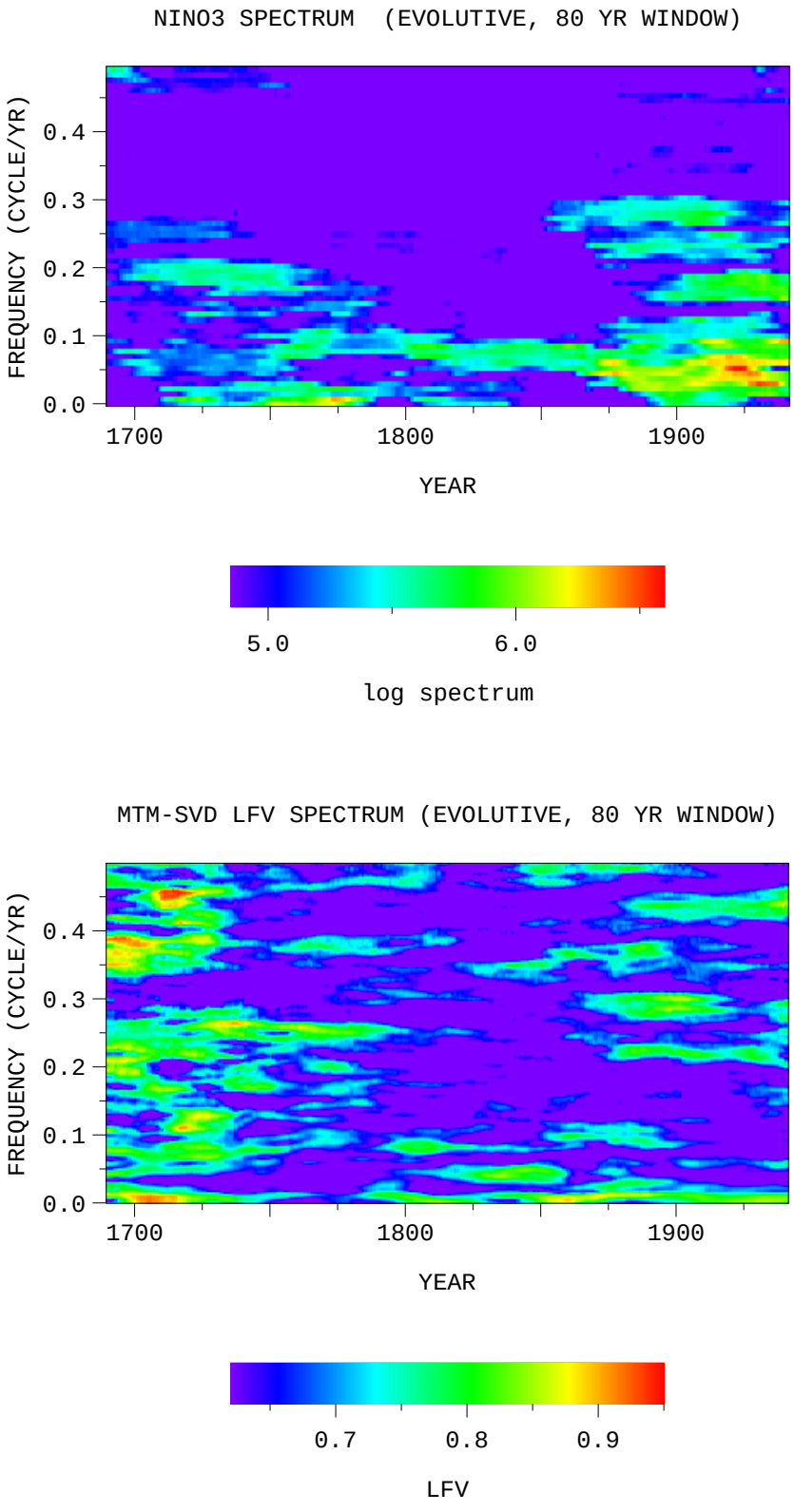

Fig. 20 Evolutive spectrum of Niño-3 index (top) and evolutive multivariate spectrum of global temperature fields (see text for methodological details) for the period 1650–1980, employing an 80-year moving window through time.

Frequency domain behavior

In this section, we investigate the frequency domain properties of the reconstructed history of ENSO and its large-scale teleconnections. A detailed study of the instrumental global temperature record for changes in the frequency and amplitude characteristics of ENSO and its large-scale teleconnections has been recently undertaken by Park and Mann (1998). Possible amplitude and frequency modulation of ENSO on longer timescales has been investigated in previous studies based on univariate (Michaelsen 1989; Meko 1992; Dunbar et al. 1994) and multivariate (Bradley et al. 1994) spectral analyses of ENSO-sensitive proxy data. Here, we analyze the reconstructions described in earlier sections to investigate low-frequency amplitude and frequency modulation of interannual variability, and the characteristics of decadal and longer timescale changes in the base state of ENSO. We analyze long-term changes in the frequency domain aspects of El Niño and the global ENSO signal based on the evolutive spectrum of the reconstructed Niño-3 index (Fig. 20, top; calculated based on the "multitaper method"; see Thomson 1982; Park et al. 1987; Mann and Lees 1996) and the evolutive multivariate spectrum of the global temperature field (Fig. 20, bottom; based on the "MTM-SVD" method of Mann and Park 1996, 1998; see also Rajagopalan et al. 1998; Tourre et al. 1998), respectively. In both cases, we employ an 80-year moving window in time to investigate multidecadal amplitude modulation in ENSO and its global teleconnections. Similar results are obtained for 50- or 100-year window choices.

A general tendency towards relatively higher-frequency interannual variability during the past few centuries (e.g., from 5- to 7-year period, to 4- to 5-year period) has been argued for in previous proxy ENSO studies (e.g., Dunbar et al. 1994; Michaelsen 1989; Diaz and Pulwarty 1994; Knutson et al. 1997). Such a trend is, arguably, evident in the evolutive spectral analysis of the Niño-3 index (Fig. 20, top). Frequency modulation of ENSO is not necessarily a fingerprint of anthropogenic climate change (see Knutson et al. 1997) and is consistent with natural variability in models of ENSO (Zebiak and Cane 1991; Knutson et al. 1997). What is more striking in our analysis, however, is not the frequency modulation, but rather the strong amplitude modulation, of the variability. There is evidence for relatively enhanced interdecadal variance in the reconstructed Niño-3 series during the twentieth century, and relatively enhanced secular variance during the late eighteenth century (Fig 20). The most pronounced amplitude modulation, however, is the clear breakdown in interannual variability during the early and mid-nineteenth century in both the Niño-3 index (Fig. 20, top) and the global temperature field (Fig. 20, bottom). This latter behavior in the Niño-3 index is consistent with the evolutive spectral analysis of the Galapagos coral $d^{18}O$ record (Dunbar et al. 1994) and time series waveform decompositions of SOI reconstructions (Stahle et al. 1998), both of which show weakened interannual variability during this period. This amplitude modulation is intriguing from the standpoint of possible external forcing. This period is also the coldest during the interval examined here in terms of NH mean temperature, associated with the "Maunder Minimum" period of relatively low apparent levels of solar irradiance, and preceding the marked twentieth-century greenhouse gas increases (see MBH98, Fig. 7). This coincidence suggests the possibility that interannual ENSO variability is a feature of a relatively warm climate. If this is the case, we might expect accelerated greenhouse forcing to increase the amplitude of interannual ENSO variability. On the other hand, there may also be an upper limit on the global temperature regime within which interannual ENSO variability can reside. The latter scenario is hinted at by the experiments of Knutson et al. (1997), which explored the response of a low-resolution version of the Geophysical Fluid Dynamics Laboratory (GFDL) coupled model to CO_2

forcing, and showed a decrease in the amplitude of interannual ENSO-like variability in an enhanced greenhouse climate (Knutson et al. 1997. We note, however, that other models—e.g., Zebiak and Cane 1991; Meehl and Branstator 1992—do not show such a response). Furthermore, Goddard and Graham (1998) point out that the interannual delayed oscillatory mechanism appears to have broken down in describing the more trendlike ENSO-related variability of the 1990s.

The primary differences between the evolutive Niño-3 and multivariate global temperature spectra (Fig. 20) are at the quasi-biennial and decadal-to-secular frequencies. The quasi-biennial signal appears to be associated with extratropical features largely unrelated to ENSO (see, e.g., Mann and Park 1994, 1996), while the multidecadal (secular within the context of an 80-year window) global variations are associated with the North Atlantic multidecadal pattern discussed earlier (see, e.g., Delworth et al. 1993, 1997; Kushnir 1994; Mann et al. 1995; Mann and Park 1994, 1996). The interdecadal (15–30) year signal which intermittently appears in both the Niño-3 and global multivariate spectra is associated with interdecadal ENSO-like variability that has been established in previous analyses of multiproxy data (Mann et al. 1995), and which is discussed in more detail below. As was noted earlier, the reconstructed Niño-3 index has slightly exaggerated power at decadal and lower frequencies in the twentieth century, relative to the instrumental Niño-3 index (see Fig. 10). The amplitude of decadal, relative to interannual, power may thus be somewhat exaggerated in the reconstructed Niño-3 index.

To illustrate the fundamental differences referred to earlier in the spatial pattern of the interannual ("true") ENSO signal, and the decadal ENSO-like signal, we reconstruct a typical oscillatory episode of the roughly 4- to 5-year (Fig. 21) and roughly 20- to 25-year (Fig. 22) global temperature signals based on the MTM-SVD method described by Mann and Park (1994; 1996; 1998). The primary departure of the interdecadal pattern from the ENSO pattern is the relatively subdued amplitude in the tropical Pacific, and a cooling (rather than warming) influence over both the North American and tropical Atlantic sectors coincident with warm eastern tropical Pacific (i.e., El Niño) conditions. The relative prominence of the decadal-scale ENSO pattern during the early nineteenth century thus appears to explain the unusual Pacific North American and Atlantic teleconnection pattern commented on earlier (Fig. 19). Possible origins and extratropical-tropical connections that may describe the decadal signal (and its possible relationship with ENSO) have been widely discussed elsewhere based on analyses of twentieth-century instrumental data (Trenberth 1990; Graham 1994; Trenberth and Hurrell 1994; Mann and Park 1994, 1996; Goddard and Graham 1998; Park and Mann 1998), long-term proxy climate indicators (Mann et al. 1995), and modeling experiments (Latif and Barnett 1994; Graham 1994; Gu and Philander 1997).

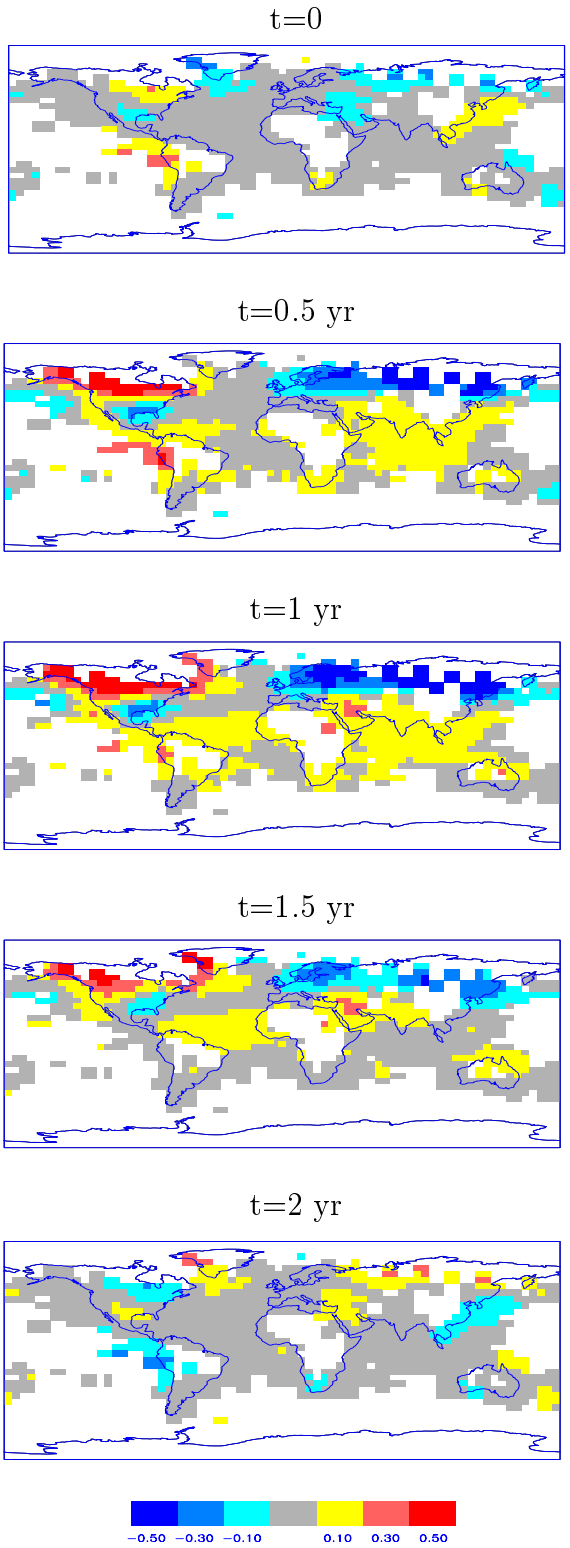

Fig. 21 Canonical pattern of the interannual ENSO signal in the temperature reconstructions as it evolves over half of a typical (roughly 4-year period) cycle.

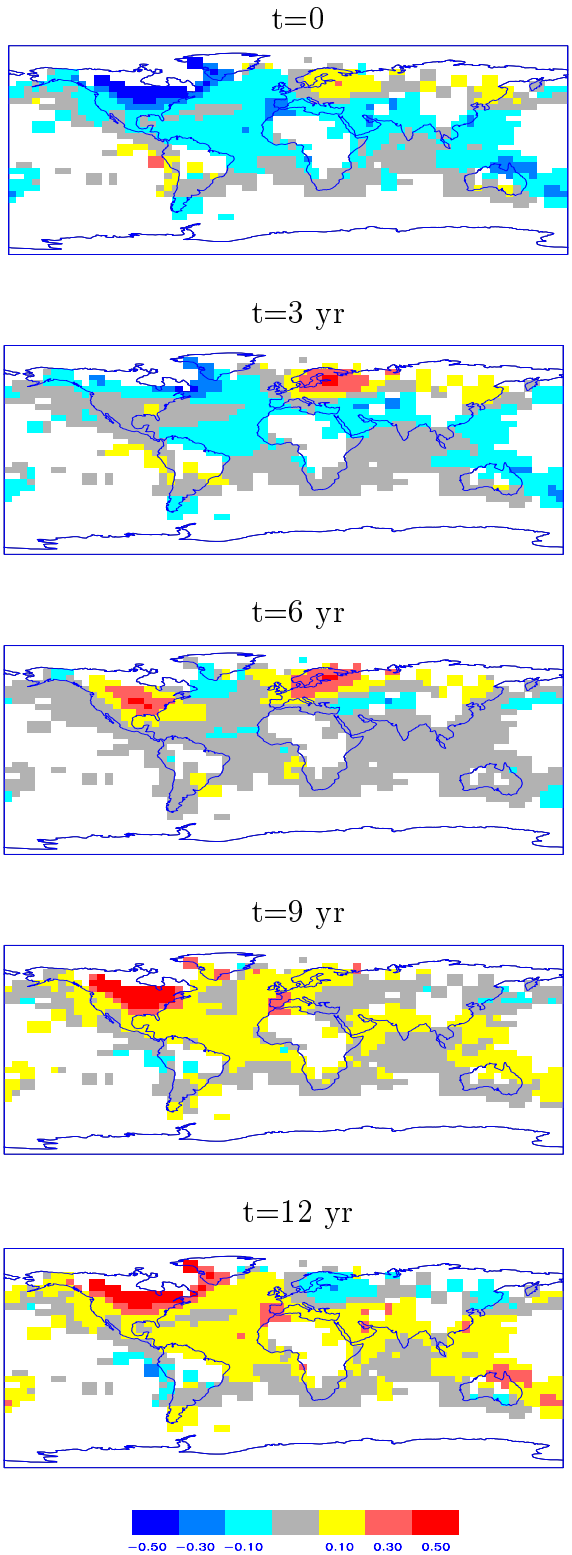

Fig. 22 Canonical pattern of the interdecadal ENSO-like signal in the temperature reconstructions as it evolves over half of a typical cycle. The cycle length is variable from about a16- to 25-year period, with the case shown corresponding to the dominant roughly 25-year period evident during the early nineteenth century.

Trends in extremes

We can further quantify variations in the rates of extreme events (e.g., both large El Niños and La Niñas) commented upon earlier, by looking at how frequencies of occurrences of anomalous events have changed over time in our Niño-3 reconstructions. Because the variance properties appear to be homogeneous back in time (the resolved variance in our Niño-3 reconstructions is a roughly constant ~40% back in time; see Table 3, and also the error bars in Fig. 17), we consider it reasonable to examine the changes in the distribution—at least the second-order statistics—back in time. Figure 23 shows the variations over time (in an 80-year moving window) in the frequency of anomalous cold and warm events (defined by an event amplitude greater than one standard deviation, based on the calibration period [1902–80] mean and variance of the instrumental Niño-3 index). The low-frequency variations in the frequency of both anomalous warm and cold events are similar to estimates of the low-frequency variations in the probability of all (weak and strong) warm events based on combined documentary, tropical ice core $d^{18}O$, and extratropical dendroclimatic-based indices of ENSO-related variability (Michaelsen and Thompson 1992). In each case, a pronounced decreasing trend in occurrences is observed from the eighteenth through mid-nineteenth century, and a pronounced increasing trend from the mid-nineteenth through early twentieth century. The unusually low incidence of anomalous warm events during the early nineteenth century, coincides closely with the breakdown of interannual variability (Fig. 20), and altered global teleconnection patterns (Fig. 19) during that period of time. Aside from the overall trend of increases in both cold and warm extremes since the mid-nineteenth century, our analysis indicates a trend towards enhanced skewness of the Niño-3 distribution during the twentieth century. The frequency of anomalous cold events has increased dramatically during the twentieth century, similar to the warm event occurrence rates of Michaelsen and Thompson (1992), while the frequency of anomalous warm events has actually decreased during the early twentieth century. Cold and warm event occurrences, otherwise, largely track each at multidecadal and longer timescales. It is interesting that this skewness of the Niño-3 distribution appears to be reversing in recent decades, owing to the recent run of anomalous warm events (see, e.g., Trenberth 1990).

The possibility that El Niño episode durations or "spell lengths" have increased in association with global warming has been highlighted by the recent study of Trenberth and Hoar (1996; see also the follow-ups by Rajagopalan et al. 1997; Trenberth and Hoar 1997), which emphasized the unusually long nature of the 1990–95 warm episode. We investigate how unusual such a warm spell is within the context of our several centuries–long reconstructions. Figure 24 shows the frequency of 5-year-long "warm spells," defined as the number of distinct, uninterrupted stretches of positive Niño-3 values per 80-year period, as a function of time. The most dramatic feature is the trend towards far fewer long "warm spells" during the twentieth century. In this context, the 1990–95 event is particularly striking, occurring during the period of recent increases in warm event frequencies (Fig. 23) and anomalous warm events (Fig. 17). However, this spell does not appear especially unusual when viewed in the context of certain previous periods, such as the early nineteenth century, during which there were between three and five 5-year-long warm events within the confines of our estimated uncertainties. This finding is supported by an independent proxy-based study by Allan and D'Arrigo (1998), which provides evidence for numerous "persistent" warm episodes in past centuries. It is worth emphasizing that the early nineteenth-century period associated with the greatest probability of warm spells is associated, as was commented upon earlier, with the coldest global temperatures back to 1650, and an apparent

breakdown of interannual ENSO variability. The unusually protracted 1990–95 event may, in turn, be signaling a breakdown of interannual ENSO variability at the "warm global temperature" boundary of its dynamical regime.

Selected ENSO events

Here, we look at global patterns for eight selected warm and cold ENSO years. Figure 25 shows the patterns for various strong (S) and very strong (VS) category El Niño years indicated by the QN92 chronology and associated with warm values of our reconstructed Niño-3 index. The correspondence between our reconstructed Niño-3 index and the QN92 chronology is far from perfect—many QN92 warm events do not correspond to warm reconstructed Niño-3 values, and many warm reconstructed Niño-3 years do not correspond to QN92 warm events. We suspect that the discrepancies result from a combination of the uncertain nature of our reconstructions (which, after all, resolve only about 40% of the instrumental Niño-3 variance for the calibration period; Table 3) and possible weaknesses in the QN92 chronology itself (note, for example, the imperfect correspondence between the QN92 warm event chronology and the negative SOI peaks during the verification period; Fig. 13). However, we note that the correspondence between our reconstruction and the QN92 warm event chronology is significant well above the 99% confidence level based on Monte Carlo permutation tests (Table 3).

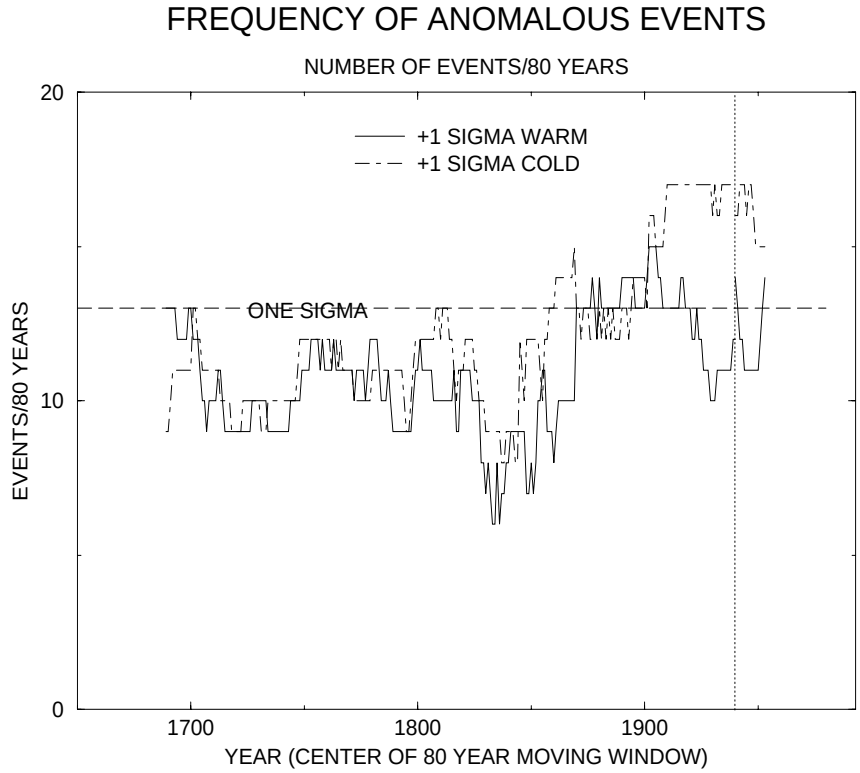

Fig. 23 Frequency of extreme warm or cold ENSO events per 80-year period, based on the reconstructed Niño-3 index from 1650–1980. The number of 1 sigma "outliers" expected for a Gaussian distribution with the same variance as the observed distribution during the 1902–80 calibration period is shown (horizontal dashed line) for comparison. Recent results are shown (boundary marked by the vertical line) based on the instrumental Niño-3 index available from 1902–1993.

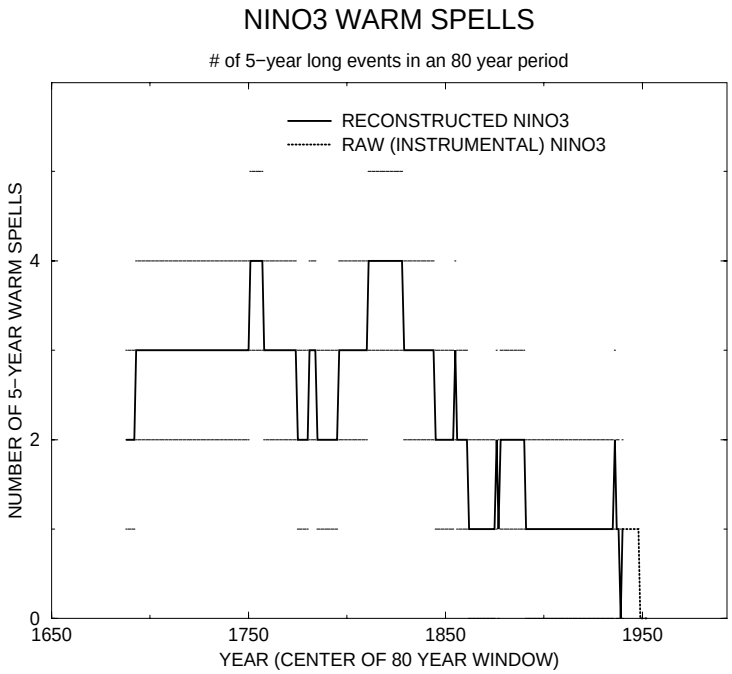

Fig. 24 Frequency of unusually (5-year) long warm ENSO "spells" per 80-year period, for the reconstructed Niño-3 index from 1650–1980 (solid curve). Recent results are shown (dotted curve) based on the instrumental Niño-3 index available from 1902–93; 1 standard uncertainty limits are indicated (dashed) for the estimated number of warm spells in a given 80-year period. These limits were determined from Monte Carlo simulations taking into account the uncertainties in the Niño-3 reconstruction itself (see Fig. 17).

The pattern for 1652 (shown, as in all events, relative to a zero reference corresponding to the 1902–80 climatology) indicates warming in the Niño-3 region, but an unusual lack of warm anomalies along Pacific coastal South and Central America. This is similarly true for 1804 and 1828, which show cooling or neutral anomalies in most areas other than the Niño-3 region, largely because these events are superimposed on the considerably cold global baseline conditions of the early nineteenth century discussed earlier. The 1828 pattern, which also falls in the center of the 1801–50 period earlier noted (Fig. 19) for its unusual global ENSO correlation pattern, is particularly atypical. The 1877 and 1884 events exhibit particularly strong tropical eastern Pacific warm tongue anomalies, which are more typical of the twentieth century (e.g., Fig. 11) pattern. In summary, the patterns of different reconstructed ENSO years are quite variable—this is probably due in part to the inherent event-to-event noise, in part to the obscuring influence of other processes influencing global temperatures, and in part to real changes in ENSO teleconnections over time (e.g., Fig. 19).

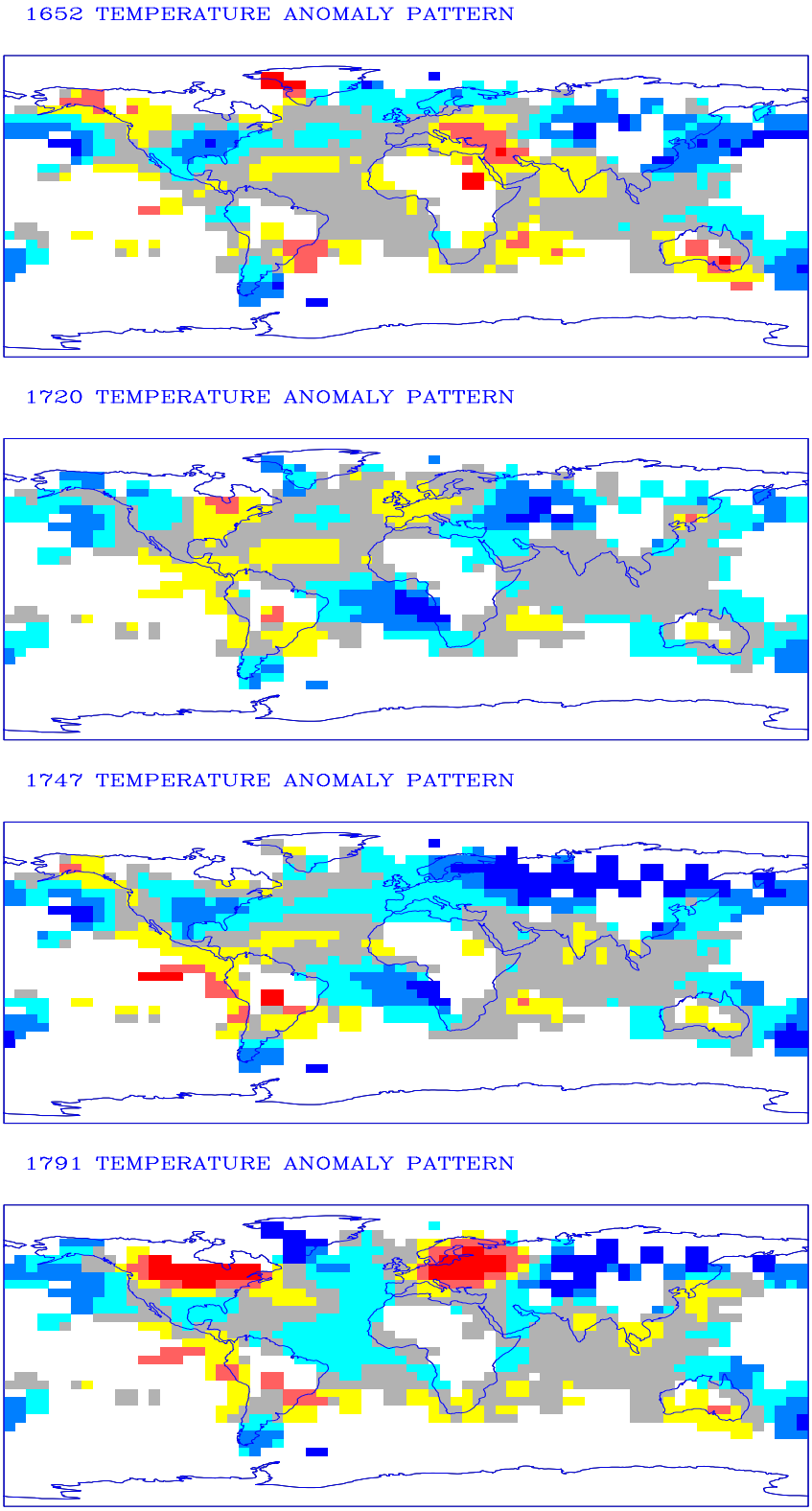

Fig. 25a Global temperature anomaly patterns for selected QN92 documented strong (S) and very strong (VS) El Niño years. (a) 1652, (b) 1720, (c) 1747, (d) 1791. Color scale (same as in Fig. 19) indicates anomalies in Celsius relative to 1902–80 climatological mean.

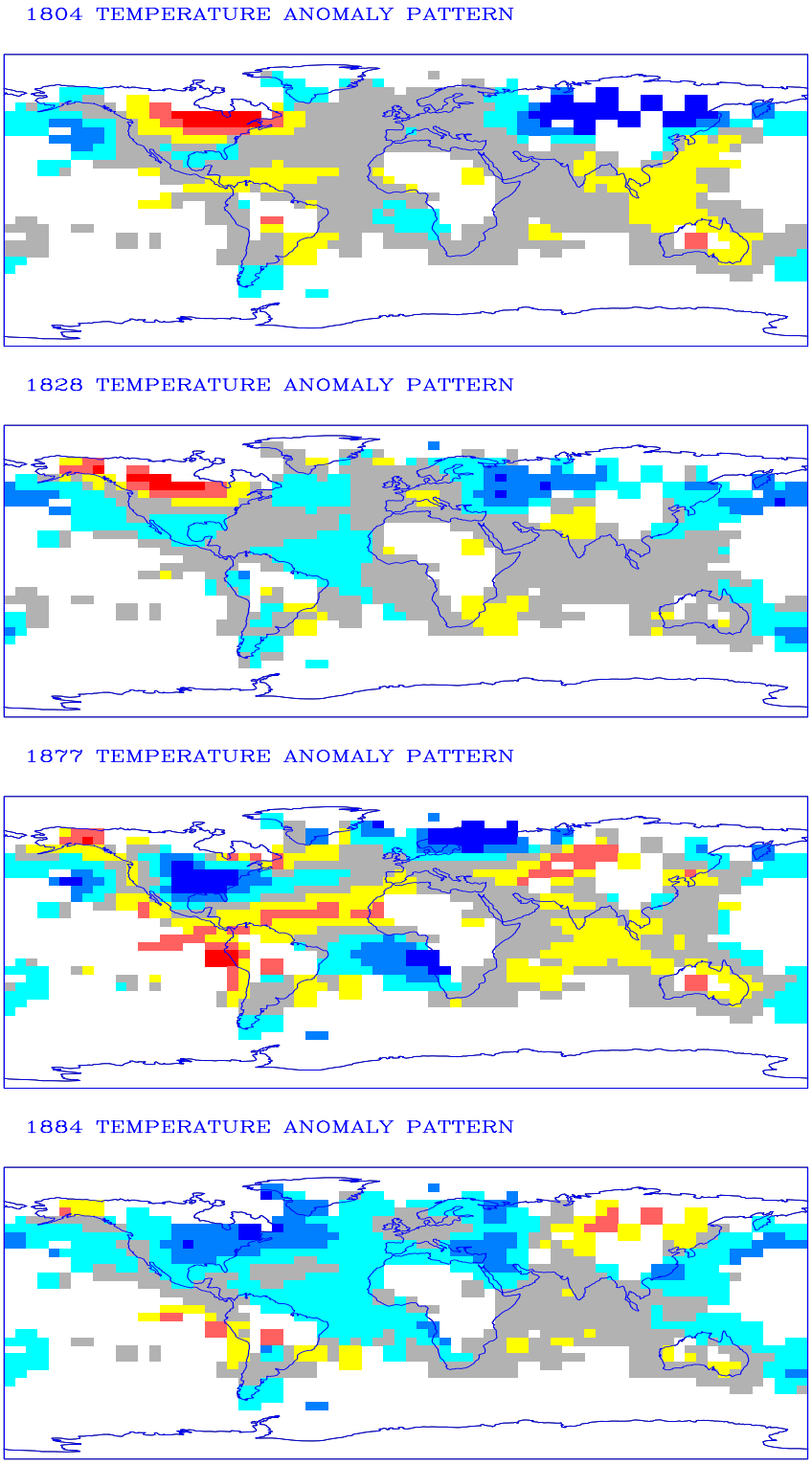

Fig. 25a Global temperature anomaly patterns for selected QN92 documented strong (S) and very strong (VS) El Niño years. (a) 1804, (b) 1828, (c) 1877, (d) 1884. Color scale (same as in Fig. 19) indicates anomalies in Celsius relative to 1902–80 climatological mean.

Figure 26 shows global temperature anomaly patterns for two selected cold events during the eighteenth century. Note that the patterns depart significantly from the mirror images of warm events such as are shown in Figure 25, in large part because of the colder climatology of the period. For example, neutral conditions in the central North Pacific relative to the twentieth-century climatology would actually correspond to more familiar warm conditions in the region if plotted relative to the colder eighteenth-century climatology. There is no independent historical corroboration of cold events, as the QN92 index documents only El Niño, and not La Niña, episodes. The cold events typically, as we would expect, fall between QN92 warm events, and frequently right after warm events. For example, the notable 1732 and 1777 reconstructed cold events shortly follow the 1728 VS and 1775 S warm events, respectively. The eighteenth century was a time of relatively pronounced interannual variability in Niño-3 (see Fig. 20), so we might tend to believe that the delayed oscillator mechanism was particularly active at this time. Hence, it is reasonable to conclude that strong warm events should tend to be followed by particularly strong cold events during this period.

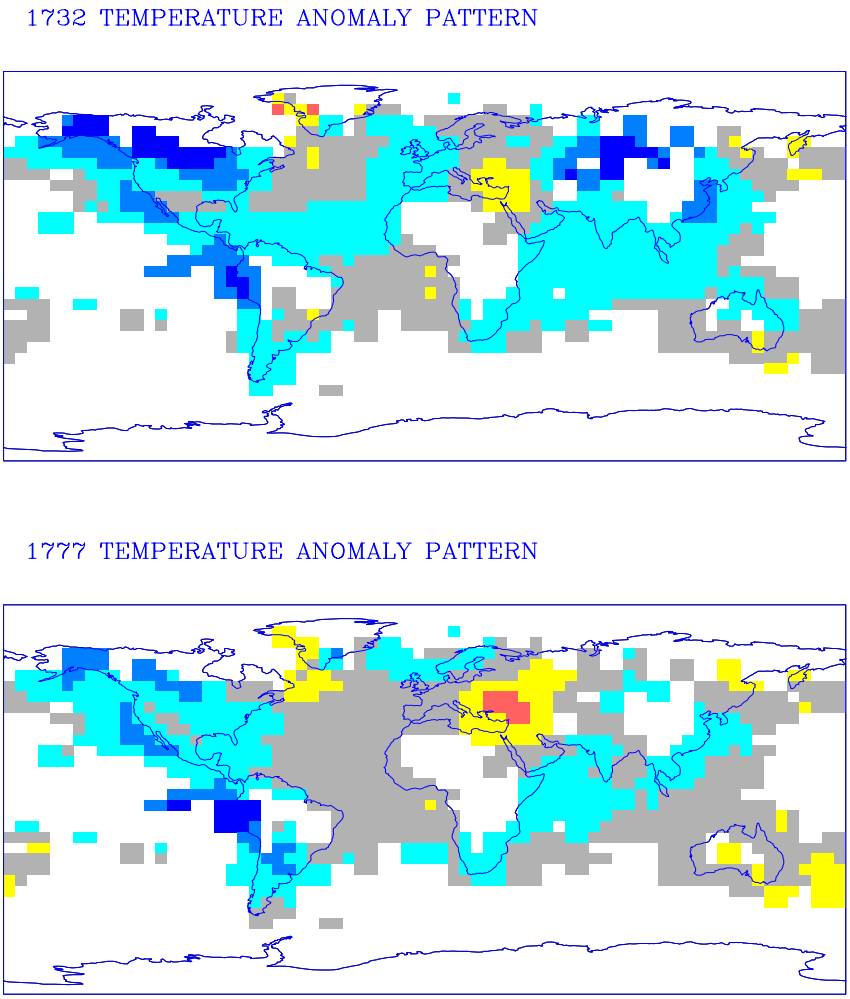

Fig. 26 Global temperature anomaly patterns for two reconstructed cold ENSO (La Niña) years. (i) 1732, (ii) 1777. Conventions are as in Figure 25.

Conclusions

The multiproxy-based reconstructions of El Niño and its large-scale patterns of influence described in this chapter provide insight into a number of issues related to ENSO, including its natural variability, and varying large-scale teleconnections on multidecadal and century timescales. Relationships with global or hemispheric mean temperatures are also evident, as are possible relationships with natural and external forcing of climate, including anthropogenic factors. Certain ENSO-related patterns and features appear to have exhibited significant trends during the twentieth century, although classic ENSO indices show only modest warming trends in comparison with the dramatic warming trend in hemispheric and global temperature during the past century. There is some evidence that a pattern associated with negative tropical feedbacks may be abating an El Niño–like warming trend in the tropical Pacific.

Equally interesting in the climate reconstructions is evidence of changes in the amplitude of interannual ENSO variability, global teleconnections of ENSO, and the amplitude and frequency of extremes. For example, the incidence of large warm and cold events appears to have increased during the past century, while the frequency of long warm ENSO spells has decreased. There is evidence, however, that some of these trends may be reversing during the most recent decades. The breakdown of interannual ENSO variability during the nineteenth century appears to have had particularly significant impacts on the incidence of extremes and on global teleconnection patterns of ENSO during that period. We find some support for the proposition that this breakdown may have been associated with the same external forcings that led to generally cold global temperatures at the time. This period may thus provide an analog for the behavior of ENSO and the possible breakdown of typical mechanisms of ENSO variability under the impacts of external—including anthropogenic—forcing of climate.

As increasingly rich networks of high-quality, seasonally resolved proxy data become available, both global temperature pattern and ENSO-scale reconstructions should be possible with considerably reduced uncertainties. Of particular utility for ENSO-scale reconstruction will be the availability of a greater number of well-dated coral isotopic indicators in the tropical Pacific to supplement the sparse existing network. With reduced uncertainties, indices of past ENSO variability should allow the unusual 1982/1983 and 1997/1998 warm events, and protracted 1990–95 “warm spell” to be placed in a proper longer-term perspective. With such a perspective, we should be better able to assess whether or not these seemingly anomalous recent events represent significant and potentially anthropogenic-related climate changes.

Acknowledgments

We are indebted to Rosanne D'Arrigo, David Fisher, Gordon Jacoby, Judith Lean, Alan Robock, David Stahle, Charles Stockton, Eugene Vaganov, Ricardo Villalba, and the numerous contributors to the International Tree-Ring Data Bank for many of the proxy data series used in this study. We thank Mike Dettinger for a thoughtful and thorough review of the manuscript. We are also grateful to Frank Keimig, Martin Munro, and Richard Holmes for their technical assistance. This work was supported by the National Science Foundation and the Department of Energy. M.E.M. acknowledges support through the Alexander Hollaender Distinguished Postdoctoral Research Fellowship program of the U.S. Department of Energy. This work is a contribution to the

Analysis of Rapid and Recent Climatic Change (ARRCC) project, sponsored by the National Science Foundation and the U.S. National Oceanic and Atmospheric Administration.

References

Allan, R., and D'Arrigo, R.D., 1998: "Persistent" ENSO sequences: How unusual was the 1990–1995 El Niño? *Holocene*, in press.

Allan, R., Lindesay, J., and Parker, D., 1996: *El Niño Southern Oscillation and Climate Variability*. CSIRO Publishing, Melbourne.

Angell, J.K., 1990: Variation in global tropospheric temperature after adjustment for the El Niño influence, 1958–1989. *Geophysical Research Letters*, **17**, 1093–1096.

Barnett, T.P., Santer, B., Jones, P.D., and Bradley, R.S., 1996: Estimates of low frequency natural variability in near-surface air temperature. *Holocene*, **6**, 255–263.

Barnston, A.G., and Livezey, R.E., 1987: Classification, seasonality and persistence of low-frequency atmospheric circulation patterns. *Monthly Weather Review*, **115**, 1083–1126.

Boninsegna, J.A., 1992: South American dendroclimatological records. *In: Climate Since A.D. 1500*, Bradley, R.S., and Jones, P.D. (eds.), Routledge, 246–268.

Bradley, R.S., 1996: Are there optimum sites for global paleotemperature reconstruction? *In: Climatic Variations and Forcing Mechanisms of the Last 2000 Years*, Jones, P.D., Bradley, R.S., and Jouzel, J. (eds.), Springer-Verlag, 603–624.

Bradley, R.S., and Jones, P.D., 1993: 'Little Ice Age' summer temperature variations: Their nature and relevance to recent global warming trends. *Holocene*, **3**, 367–376.

Bradley, R.S., Mann, M.E., and Park, J., 1994: A spatiotemporal analysis of ENSO variability based on globally distributed instrumental and proxy temperature data. *EOS Supplement*, **75**, 383.

Briffa, K.R., *et al*., 1992a: Fennoscandian summers from AD 500: Temperature changes on short and long timescales. *Climate Dynamics*, **7**, 111–119.

Briffa, K.R., Jones, P.D., Schweingruber, F.H., 1992b: Tree-ring density reconstructions of summer temperature patterns across western North America since 1600. *Journal of Climate*, **5**, 735–753.

Briffa, K.R., Jones, P.D., Schweingruber, F.H., Shiyatov, S.G., and Cook, E.R., 1995: Unusual twentieth-century summer warmth in a 1000-year temperature record from Siberia. *Nature*, **376**, 156–159.

Cane, M., et al., 1997: Twentieth-century sea surface temperature trends. *Science*, **275**, 957–960.

Chang, P., Ji, L., Li, H., and Flugel, M., 1996: Chaotic dynamics versus stochastic processes in El Niño–Southern Oscillation in coupled ocean-atmosphere models. *Physica D.*, **98**, 301–320.

Chang, P., Ji, L., and Li, H., 1997: A decadal climate variation in the tropical Atlantic Ocean from thermodynamic air-sea interactions. *Nature*, **385**, 516–518.

Cleaveland, M.K., Cook, E.R., and Stahle, D.W., 1992: Secular variability of the Southern Oscillation detected in tree-ring data from Mexico and the southern United States. *In: El Niño: Historical and Paleoclimatic Aspects of the Southern Oscillation*, Diaz, H.F., and Markgraf, V. (eds.), Cambridge University Press, Cambridge, 271–291.

Cole, J., and Cook, E., 1997: The coupling between ENSO and U.S. drought: How stable is it over the past century? *EOS Supplement*, **78**.

Cole, J.E., Fairbanks, R.G., and Shen, G.T., 1993: Recent variability in the Southern Oscillation: Isotopic results from a Tarawa atoll coral. *Science*, **260**, 1790–1793.

Cook, E.R., et al., 1991: Climatic change in Tasmania inferred from a 1089-year tree-ring chronology of Huon pine. *Science*, **253**, 1266–1268.

Cook, E.R., Briffa, K.R., and Jones, P.D., 1994: Spatial regression methods in dendroclimatology: A review and comparison of two techniques. *International Journal of Climatology*, **14**, 379–402.

Cook, E.R., Briffa, K.R., Meko, D.M., Graybill, D.A., and Funkhouser, G., 1995: The 'segment length' curse in long tree-ring chronology development for paleoclimatic studies. *Holocene*, **5**, 229–237.

D'Arrigo, R.D., Cook, E.R., Jacoby, G.C., and Briffa, K.R., 1993: NAO and sea surface temperature signatures in tree-ring records from the North Atlantic sector. *Quaternary Science Review*, **12**, 431–440.

Delworth, T.D., and Mann, M.E., 1998: Observed and Simulated Multidecadal Variability in the North Atlantic. (Submitted).

Delworth, T.D., Manabe, S., and Stouffer, R.J., 1993: Interdecadal variations of the thermohaline circulation in a coupled ocean-atmosphere model. *Journal of Climate*, **6**, 1993–2011.

Delworth, T.D., Manabe, S., and Stouffer, R.J., 1997: Multidecadal climate variability in the Greenland Sea and surrounding regions: A coupled model simulation. *Geophysical Research Letters*, **24**, 257–260.

Diaz, H.F., and Markgraf, V., 1993: *El Niño: Historical and Paleoclimatic Aspects of the Southern Oscillation.* Cambridge University Press, Cambridge, 476pp.

Diaz, H.F., and Pulwarty, R.S., 1994: An analysis of the time scales of variability in centuries-long ENSO-sensitive records in the last 1000 years. *Climatic Change*, **26**, 317–342.

Dunbar, R.B., Wellington, G.M., Colgan, M.W., and Glynn, P.W., 1994: Eastern Pacific sea surface temperature since 1600 A.D. The $d^{18}O$ record of climate variability in the Galapagos corals. *Paleoceanography*, **9**, 291–315.

Fisher, D.A., et al., 1996: Inter-comparison of ice core delta O-18 and precipitation records from sites in Canada and Greenland over the last 3500 years and over the last few centuries in detail using EOF techniques. *In: Climatic Variations and Forcing Mechanisms of the Last 2000 Years,* Jones, P.D., Bradley, R.S., and Jouzel, J., Springer-Verlag, Heidelberg, 297–328.

Fisher, D.A., et al., 1998: Penny ice cap cores, Baffin Island, Canada, and the Wisconsin Foxe Dome connection: Two states of Hudson Bay ice cover. *Science*, **279**, 692–965.

Folland, C.K., Parker, D.E., and Kates, F.E., 1984: Worldwide marine temperature fluctuations 1856–1981. *Nature*, **310**, 670–673.

Fritts, H., 1991: *Reconstructing Large-Scale Climatic Patterns from Tree Ring Data*, University of Arizona Press Tucson.

Fritts, H.C., and Shao, X.-M., 1992: *In: Climate Since A.D. 1500*, Bradley, R.S., and Jones, P.D. (eds.), Routledge, 269–294.

Fritts, H.C., Blasing, T.J., Hayden, B.P., and Kutzbach, J.E., 1971: Multivariate techniques for specifying tree-growth and climate relationships and for reconstructing anomalies in paleoclimate. *Journal of Applied Meteorology*, **10**, 845–864.

Goddard, L., and Graham, N.E., 1998: El Niño in the 1990s. *Journal of Geophysical Research*, **102**, 10423–10436.

Graham, N.E., 1994: Decadal-scale variability in the tropical and North Pacific during the 1970s and 1980s: Observations and model results. *Climate Dynamics*, **10**, 135–162.

Gu, D., and Philander, S.G.H., 1997: Interdecadal climate fluctuations that depend on exchanges between the tropics and extratropics. *Science*, **275**, 805–807.

Guiot, J., 1988: The combination of historical documents and biological data in the reconstruction of climate variations in space and time. *Palaeoklimaforschung*, **7**, 93–104.

Halpert, M.S., and Ropelewski, C.F., 1992: Surface temperature patterns associated with the Southern Oscillation. *Journal of Climate*, **5**, 577–593.

Heiss, G.A., 1994: Coral reefs in the Red Sea: Growth, production and stable isotopes. GEOMAR Report 32, 1–141.

Hughes, M.K., and Diaz, H.F., 1994: Was there a "Medieval Warm Period" and if so, where and when? *Climatic Change*, **26**, 109–142.

Hughes, M.K., Vaganov, E.A., Shiyatov, S.A., Touchan, R., and Funkhouser, G., 1998: Twentieth-century summer warmth in northern Yakutia in a 600-year context. Submitted.

Hurrell, J.W., 1995: Decadal trends in the North Atlantic Oscillation, regional temperatures and precipitation. *Science*, **269**, 676–679.

Intergovernmental Panel on Climate Change (IPCC), 1995: *Climate Change 1995: The Science of Climate Change*, Houghton, J.T., et al. (eds.), Cambridge University Press, Cambridge.

Jacoby, G.C., and D'Arrigo, R., 1989: Reconstructed Northern Hemisphere annual temperature since 1671 based on high-latitude tree-ring data from North America. *Climatic Change*, **14**, 39–59.

Jacoby, G.C., and D'Arrigo, R.D., 1990: Teak: A tropical species of large-scale dendroclimatic potential. *Dendrochronologia*, **8**, 83–98.

Jacoby, G.C., D'Arrigo, R.D., and Tsevegyn, D., 1996: Mongolian tree rings and 20th-century warming. *Science*, **9**, 771–773.

Jin, F.F, Neelin, J.D., and Ghil, M., 1994: El Niño on the devil's staircase: Annual subharmonic steps to chaos. *Science*, **264**, 70–72.

Jones, P.D., 1989: The influence of ENSO on global temperatures. *Climate Monitor*, **17**, 80–89.

Jones, P.D., 1998: It was the best of times, it was the worst of times. *Science*, **280**, 544–545.

Jones, P.D., and Bradley, R.S., 1992: *In: Climate Since A.D. 1500*, Bradley, R.S., and Jones, P.D. (eds.), Routledge, 246–268.

Jones, P.D., and Briffa, K.R., 1992: Global surface air temperature variations during the 20th century: Part I–Spatial, temporal and seasonal details. *Holocene*, **1**, 165–179.

Kameda, T., Narita, H., Shoji, J., Nishio, F., and Watanabe, O., 1992: *Proc. International Symposium on the Little Ice Age Climate*, Tokyo Metropolitan University, Tokyo, Japan.

Kaplan, A., *et al.*, 1998: Analyses of global sea surface temperature 1856–1991. *Journal of Geophysical Research*, in press.

Knutson, T., Manabe, S., and Gu, D., 1997: Simulated ENSO in a global coupled ocean-atmosphere model: Multidecadal amplitude modulation and CO_2 sensitivity. *Journal of Climate*, **10**, 138–161.

Kushnir, Y., 1994: Interdecadal variations in North Atlantic sea surface temperature and associated atmospheric conditions. *Journal of Climate*, **7**, 141–157.

Latif, M., and Barnett, T.P., 1994: Causes of decadal climate variability over the North Pacific and North America. *Science*, **266**, 634–637.

Lau, N.C., and Nath, M.J., 1994: A modeling study of the relative roles of tropical and extratropical SST anomalies in the variability of the global atmosphere-ocean system. *Journal of Climate*, **7**, 1184–1207.

Lau, N.C., Philander, S.G.H., and Nath, M.J., 1992: Simulation of ENSO-like phenomena with a low-resolution coupled GCM of the global ocean and atmosphere. *Journal of Climate*, **5**, 284–307.

Linsley, B.K., Dunbar, R.B., and Mucciasone, D.A., 1994: A coral-based reconstruction of Inter-Tropical Convergence Zone variability over Central America since 1707. *Journal of Geophysical Research*, **99**, 9977–9994.

Lough, J.M., 1991: Rainfall variations in Queensland, Australia: 1891–1986. *International Journal of Climatology*, **11**, 745–768.

Manley, G., 1959: Mean temperature of Central England 1698–1952. *Quarterly Journal of the Royal Meteorological Society*, **79**, 242–261.

Mann, M.E., and Lees, J., 1996: Robust estimation of background noise and signal detection in climatic time series. *Climatic Change*, **33**, 409–445.

Mann, M.E., and Park, J., 1994: Global scale modes of surface temperature variability on interannual to century time scales. *Journal of Geophysical Research*, **99**, 25819–25833.

Mann, M.E., and Park, J., 1996: Joint spatio-temporal modes of surface temperature and sea level pressure variability in the Northern Hemisphere during the last century. *Journal of Climate*, **9**, 2137–2162.

Mann, M.E., and Park, J., 1998: Oscillatory spatiotemporal signal detection in climate studies: A multiple-taper spectral domain approach. *Advances in Geophysics*, in press.

Mann, M.E., Park, J., and Bradley, R.S., 1995: Global interdecadal and century-scale oscillations during the past five centuries. *Nature*, **378**, 266–270.

Mann, M.E., Bradley, R.S., and Hughes, M.K., 1998a: Global-scale temperature patterns and climate forcing over the past six centuries. *Nature*, **392**, 779–787.

Mann, M.E., Bradley, R.S., and Hughes, M.K., 1998b: Northern Hemisphere temperatures during the past millennium: Inferences, uncertainties, and limitations. *Geophysical Research Letters.* Submitted.

Mann, M.E., Bradley, R.S., Hughes, M.K., and Jones, P.D., 1998c: Global temperature patterns. *Science*, **280**, 2029–2030.

Meehl, G.A., and Branstator, G.W., 1992: Coupled climate model simulation of El Niño/ Southern Oscillation: Implications for paleoclimate. *In: El Niño: Historical and Paleoclimatic Aspects of the Southern Oscillation*, Diaz, H.F., and Markgraf, V. (eds.), Cambridge University Press, Cambridge, 69–91.

Meehl, G.A., and Washington, W.M., 1996: El Niño–like climate change in a model with increased atmospheric CO_2 concentrations. *Nature*, **382**, 56–60.

Meko, D., 1992: Spectral properties of tree-ring data in the United States Southwest as related to El Niño/Southern Oscillation. *In: El Niño: Historical and Paleoclimatic Aspects of the Southern Oscillation*, Diaz, H.F., and Markgraf, V. (eds.), Cambridge Univ. Press, Cambridge, 349–375.

Michaelsen, J., 1989: Long-period fluctuations in El Niño amplitude and frequency reconstructed from tree-rings. *In: Aspects of Climate Variability in the Pacific and the Western Americas*, Peterson, D.H. (ed.), Geophysical Monograph 55, American Geophysical Union, Washington, D.C., 69–74.

Michaelsen, J., and Thompson, L.G., 1992: A comparison of proxy records of El Niño/Southern Oscillation. *In: El Niño: Historical and Paleoclimatic Aspects of the Southern Oscillation*, Diaz, H.F., and Markgraf, V. (eds.), Cambridge University Press, Cambridge, 7–28.

Norton, D.A., and Palmer, J.G., 1992: Dendroclimatic evidence from Australasia. *In: Climate Since A.D. 1500,* Bradley, R.S., and Jones, P.D. (eds.), Routledge, 463–482.

Ortlieb, L., 1998: The documentary historical record of El Niño events in Peru: An update of the Quinn record (sixteenth through nineteenth centuries), this volume.

Park, J., and Mann, M.E., 1998: Interannual temperature events and shifts in global temperature: A multiple wavelet correlation approach. *Earth Interactions*, in revision.

Park, J., Lindberg, C.R., and Vernon, F.L., III, 1987: Multitaper spectral analysis of high-frequency seismograms. *Journal of Geophysical Research*, **92**, 12675–12684.

Pfister, C., 1992: Monthly temperature and precipitation in central Europe from 1525–1979: quantifying documentary evidence on weather and its effects. *In: Climate Since A.D. 1500*, Bradley, R.S., and Jones, P.D. (eds.), Routledge, 118–142.

Philander, S.G.H., 1990: *El Niño, La Niña, and the Southern Oscillation*, Academic Press.

Preisendorfer, R.W., 1988: *Principal Component Analysis in Meteorology and Oceanography*, Elsevier, Amsterdam.

Quinn, W.H., and Neal, V.T., 1992: The historical record of El Niño events. *In: Climate Since A.D. 1500*, Bradley, R.S., and Jones, P.D. (eds.), Routledge, 623–648.

Quinn, T.M., Taylor, F.W., and Crowley, T.J., 1993: A 173 year stable isotope record from a tropical South Pacific coral. *Quaternay Science Reviews*, **12**, 407–418.

Quinn, T.M., Taylor, F.W., Crowley, T.J., and Link, S.M., 1996: Evaluation of sampling resolution in coral stable isotope records: A case study using monthly stable isotope records from New Caledonia and Tarawa. *Paleoceanography*, **11**, 529–542.

Rajagopalan, B., Lall, U., and Cane, M.A., 1997: Anomalous ENSO occurrences: An alternative view. *Journal of Climate*, **10**, 2351–2357.

Rajagopalan, B., Mann, M.E., and Lall, U., 1998: A multivariate frequency-domain approach to long-lead climatic forecasting. *Weather and Forecasting*, **13**, 58–74.

Schweingruber, F.H., Briffa, K.R., and Jones, P.D., 1991: Yearly maps of summer temperatures in western Europe from A.D. 1750 to 1975 and western North America from 1600 to 1982. *Vegetatio*, **92**, 5–71.

Schlesinger, M.E., and Ramankutty, N., 1994: An oscillation in the global climate system of period 65–70 years. *Nature*, **367**, 723–726.

Smith, T.M., Reynolds, R.W., Livezey, R.E., Stokes, D.C., 1996: Reconstruction of historical sea surface temperatures using empirical orthogonal functions. *Journal of Climate*, **9**, 1403–1420.

Stahle, D.W., and Cleaveland, M.K., 1993: Southern Oscillation extremes reconstructed from tree rings of the Sierra Madre Occidental and southern Great Plains. *Journal of Climate*, **6**, 129–140.

Stahle, D.W., Cleaveland, M.K., and Heher, J.G., 1988: North Carolina climate changes reconstructed from tree rings A.D. 372 to 1985. *Science*, **240**, 1517–1519.

Stahle, D.W., D'Arrigo, R.D., Krusic, P.J., Cleaveland, M.K., Cook, E.R., Allan, R.J., Cole, J.E., Dunbar, R.B., Therell, M.D., Gay, D.A., Moore, M.D., Stokers, M.A., Burns, B.T., and Thompson, L.G., 1998: Experimental dendroclimatic reconstruction of the Southern Oscillation. *Bulletin of the American Meteorological Society*, submitted.

Tarussov, A., 1992: The Arctic and Svalbard to Severnaya Zemlya: climatic reconstructions from ice cores. *In: Climate Since A.D. 1500*, Bradley, R.S., and Jones, P.D. (eds.), Routledge, 505–516.

Thomson, D. J., 1982: Spectrum estimation and harmonic analysis. *IEEE Proc.*, **70**, 1055–1096.

Thompson, L.G., 1992: Ice core evidence from Peru and China. *In: Climate Since* A.D. *1500*, Bradley, R.S., and Jones, P.D. (eds.), Routledge, 517–548.

Tourre, Y., Rajagopalan, B., and Kushnir, Y., 1998: Dominant patterns of climate variability in the Atlantic over the last 136 years. *Journal of Climate*, in press.

Trenberth, K.E., 1990: Recent observed interdecadal climate changes in the Northern Hemisphere. *Bulletin of the Americal Meteorological Society*, **71**, 988–993.

Trenberth, K.E., and Hoar, T.J., 1996: The 1990–1995 El Niño–Southern Oscillation event: Longest on record. *Geophysical Research Letters*, **23**, 57–60.

Trenberth, K.E., and Hoar, T.J., 1997: El Niño and climate change. *Geophysical Research Letters*, **24**, 3057–3060.

Trenberth, K.E., and Hurrell, J.W., 1994: Decadal atmosphere-ocean variations in the Pacific. *Climate Dynamics*, **9**, 303–319.

Tziperman, E., Stone, L., Cane, M.A., and Jarsoh, H., 1994: El Niño chaos: Overlapping of resonances between the seasonal cycle and the Pacific ocean-atmosphere oscillator. *Science*, **264**, 72–74.

Zebiak, S.E., and Cane, M.A., 1987: A model El Niño–Southern Oscillation. *Monthly Weather Review*, **115**, 2262–2278.

Zebiak, S.E., and Cane, M.A., 1991: Natural climate variability in a coupled model. *In: Greenhouse Gas–Induced Climatic Change: A Critical Appraisal of Simulations and Observations*, Schlesinger, M.E. (ed.), Elsevier, 457–469.